Nano-Micro Letters

e-ISSN 2150-5551
CN 31-2103/TB

REVIEW

https://doi.org/10.1007/s40820-024-01573-4

Cite as
Nano-Micro Lett.
(2025) 17:85

Received: 3 July 2024
Accepted: 22 October 2024

Tailoring Cathode–Electrolyte Interface for High-Power and Stable Lithium–Sulfur Batteries

Mengting Liu[1], Ling-Jiao Hu[1], Zhao-Kun Guan[1], Tian-Ling Chen[1], Xin-Yu Zhang[1], Shuai Sun[1], Ruoli Shi[1], Panpan Jing[2] ✉, Peng-Fei Wang[1] ✉

HIGHLIGHTS

- This review delves into the mechanism of the state-of-the-art lithium–sulfur batteries from a novel perspective of cathode–electrolyte interface.
- It provides extensive strategies to construct a stable cathode–electrolyte interphase layer and improve the uneven deposition of Li_2S, enhancing the stability of the interface structure.
- It proposes an in-depth and comprehensive research on how to inhibit the shuttle effect at the cathode–electrolyte interface with regard to distinct reaction pathways.

ABSTRACT Global interest in lithium–sulfur batteries as one of the most promising energy storage technologies has been sparked by their low sulfur cathode cost, high gravimetric, volumetric energy densities, abundant resources, and environmental friendliness. However, their practical application is significantly impeded by several serious issues that arise at the cathode–electrolyte interface, such as interface structure degradation including the uneven deposition of Li_2S, unstable cathode–electrolyte interphase (CEI) layer and intermediate polysulfide shuttle effect. Thus, an optimized cathode–electrolyte interface along with optimized electrodes is required for overall improvement. Herein, we comprehensively outline the challenges and corresponding strategies, including electrolyte optimization to create a dense CEI layer, regulating the Li_2S deposition pattern, and inhibiting the shuttle effect with regard to the solid–liquid–solid pathway, the transformation from solid–liquid–solid to solid–solid pathway, and solid–solid pathway at the cathode–electrolyte interface. In order to spur more perceptive research and hasten the widespread use of lithium–sulfur batteries, viewpoints on designing a stable interface with a deep comprehension are also put forth.

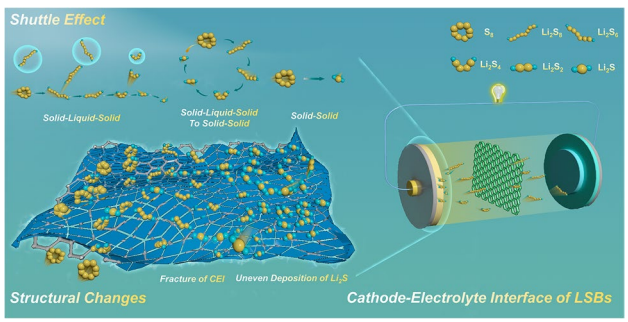

KEYWORDS Lithium–sulfur batteries; Shuttle effect; Cathode–electrolyte interface; Structural enhancement; Reaction pathway

Mengting Liu and Ling-Jiao Hu have contributed equally to this work.

✉ Panpan Jing, jingpanpan@sust.edu.cn; Peng-Fei Wang, pfwang@xjtu.edu.cn

[1] Center of Nanomaterials for Renewable Energy, State Key Laboratory of Electrical Insulation and Power Equipment, School of Electrical Engineering, Xi'an Jiaotong University, Xi'an 710049, People's Republic of China

[2] Low-Dimensional Materials and Photo/Electrochemical Technology Lab, School of Materials Science and Engineering, Shaanxi Key Laboratory of Green Preparation and Functionalization for Inorganic Materials, Shaanxi University of Science & Technology, Xi'an 710021, People's Republic of China

Published online: 04 December 2024

1 Introduction

Continuously increased demand but lack of energy has emerged as one of the most pressing issues confronting human society since the second industrial revolution [1]. Energy storage technology has flourished as a result of the tremendous growth in green energy production to offset the overconsumption of traditional fossil fuels [2–8]. Electrochemical energy storage has brought about great breakthroughs from the grid to every aspect of human life. Due to the superiorities of significant energy density and long-term cycling stability, lithium-ion batteries (LIBs) have played a vital role in most electronic portable devices since their first commercialization in 1991 by Sony Corporation [9–15]. Nevertheless, the energy density of LIBs while once regarded as high compared to capacitors and lead-acid batteries can hardly keep up with the contemporary ever-increasing energy storage demands because the theoretical specific capacities of cathodes like $LiFeO_4$, $LiCoO_2$, and $LiMn_2O_4$ are comparatively limited [16, 17]. Therefore, a number of energy storage alternatives "beyond LIBs" are investigated [18–21].

Lithium–sulfur batteries (LSBs) attracted widespread attention because of their potentially high theoretical energy density (2600 Wh kg^{-1}) outperforming times the counterpart of conventional LIBs ($LiCoO_4$:300 Wh kg^{-1}) by approximately 8.6 [6, 26, 27]. As shown in Fig. 1a, the LSBs have wider operating temperature and much lower costs than LIBs. Moreover, together with the longer driving distance, the LSBs hold greater potential in commercial applications. Since LSBs and LIBs are both lithium-based batteries, the commercial application status of LSBs still could not compare with LIBs even regarding the unique merits of LSBs [28]. What blocks the application of LSBs requires deeper thinking and the underlying reason might trace back to its distinct working principle different from that of LIBs. The rocking chair-type battery like sodium-ion battery or LIBs mainly depends on the reverse intercalation and de-intercalation of Li^+ from the cathode to anode during cycling and is therefore called a "rocking chair"-type battery [29–33]. Taking the LIB as an example with $LiCoO_2$ cathode and graphite anode (Fig. 2a), the galvanostatic charge–discharge (GCD) curves and related chemical reactions that occur at electrodes can be presented in Fig. 2b, c, respectively. In comparison, the working principle of LSBs is much more complex and trickier, which not only has great differences in reactions at different stages but also involves complex solid–liquid–solid-phase revolution in conventional reaction pathway with two plateaus (Fig. 2e, f) [34–36]. The following are the specific reaction steps. The overall chemical reaction during the discharge process can be simplified as $16Li^+ + S_8 + 16e^- \rightarrow 8Li_2S$, and it is a multi-step S reduction reaction. In stage I, S_8 is first reduced to soluble Li_2S_8. In stage II at about 2.3 V (vs. Li^+/Li), there comes the first

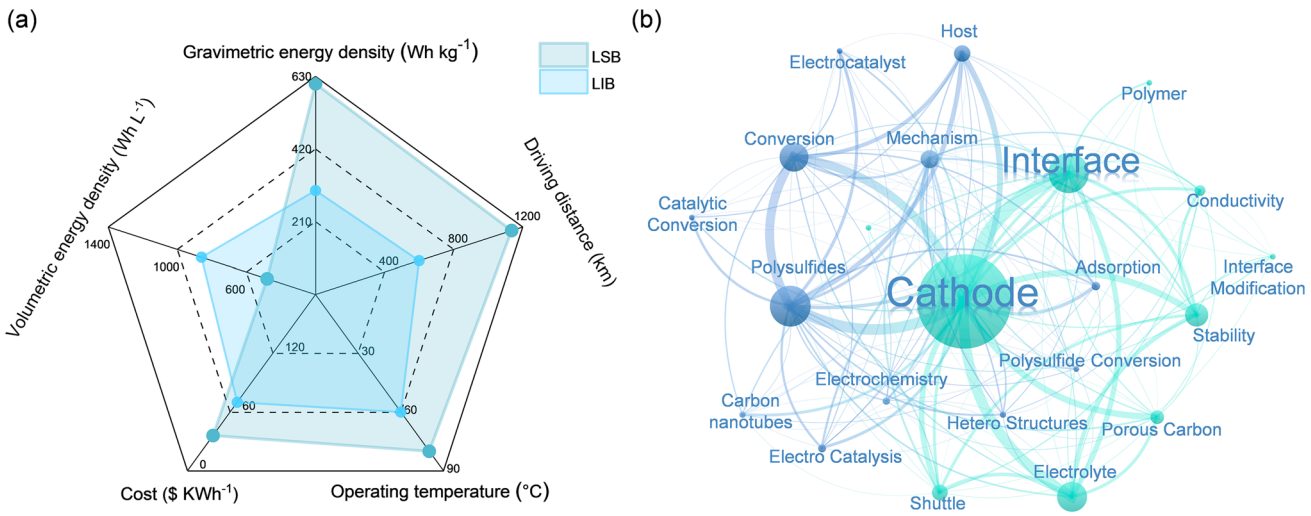

Fig. 1 **a** Radar chart comparing key parameters of LSB and LIB [6, 22–25]. **b** Network of potential challenges and strategies of cathode–electrolyte interface throughout the reports of LIBs in the past decade

https://doi.org/10.1007/s40820-024-01573-4

plateau, attributed to the reduction process from Li_2S_8 to Li_2S_6. Afterward, the Li_2S_6 is reduced to Li_2S_4. The first two stages consist of solid–liquid-phase transformation contributing to a theoretic capacity of 419 mAh g^{-1} with 4 electrons [35]. Moreover, during the first two stages the formed reduction product Li_2S_x ($4 \le x \le 8$) is all soluble and will dissolve into the electrolyte and shuttle back and forth between the cathode–electrolyte interface, separator, and the anode in the cycling process [25]. The dissolution in the first two stages is the origin of the notorious shuttle effect. In the subsequent stage III, the second plateau at about 2.1 V (vs. Li^+/Li) corresponds to the liquid–solid-phase transformation from the Li_2S_4 to the Li_2S_2 and Li_2S [37, 38]. In the last stage IV, the solid Li_2S_2 is eventually reduced to the solid Li_2S. Compared with the first two stages, stage III and stage IV with 12 electrons transfer in total contribute a capacity of 1256 mAh g^{-1}. Furthermore, it has been demonstrated that the deposition of Li_2S and the speciation of S_8 are both the rate-determining steps in the discharge and charge process, respectively, through the CV profiles [39, 40]. This sluggish kinetics might originate from its uneven deposition pattern and insolubility. Due to the density differences of Li_2S and S, the volume of the cathode will also change drastically during cycling [41–43]. In other components of LSBs, the lithium dendrites growth, anode volume expansion, and unstable solid electrolyte interphase (SEI) layer pose a threat to the anode and the uncontrollable lithium dendrites might pierce through the separator [44–47]. It has been reported that the shuttling high-order intermediate polysulfides (LiPSs) could have parasitic reactions with the lithium anode and form the insualting layer of Li_2S_2 and Li_2S to passivate and corrode the anode [48, 49]. All the issues mentioned above will cause the loss of active materials, low coulombic efficiency, capacity decline, and even safety hazards.

Over the past few years, extensive studies have been dedicated to mitigating the issues mentioned above. Firstly, various methods have been explored to enhance the conductivity of S cathodes [50]. The incorporating of conductive additives such as carbon nanotubes or graphene has proven to be an effective approach for improving electron transport [51]. In terms of the S host, researchers have favored the construction of porous framework with connected pores, effectively increasing electronic conductivity while providing a buffer space for volume expansion of S [52, 53]. Secondly, significant advancements have been made in separator technology to prevent the diffusion

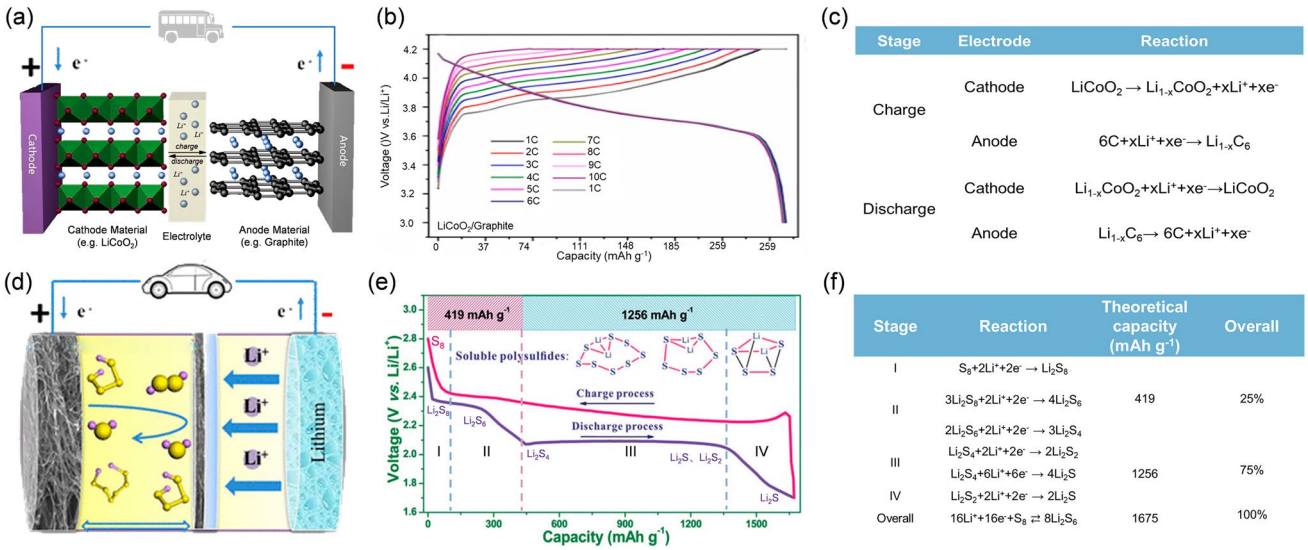

Fig. 2 **a** Schematic internal configuration illustration of LIBs. Reproduced with permission from Ref. [71], Copyright 2011, Royal Society of Chemistry. **b** GCD curves of $LiCoO_2$ cathode of LIBs. Reproduced with permission from Ref. [72], Copyright 2022, Royal Society of Chemistry. **c** Redox reactions of $LiCoO_2$ cathode of LIBs [73]. **d** Schematic internal configuration illustration of LSBs. Reproduced with permission from Ref. [74], Copyright 2018, Royal Society of Chemistry. **e** Representative GCD curves of LSBs in the ether-based electrolyte. Reproduced with permission from Ref. [75], Copyright 2020, American Chemical Society. **f** Corresponding redox reactions of S cathode of LSBs. Reproduced with permission from Ref. [76], Copyright 2022, John Wiley and Sons

of LiPSs while enabling efficient ion diffusion [54, 55]. To date, three kinds of mainstream separators, including sandwiched, janus, and composite structure, have been employed to capture the LiPSs and enhance ionic conductivity [56–59]. Thirdly, as an indispensable part in the smooth function of the LSBs, lithium alloys and carbon-based materials have been widely investigated to address dendrite formation and low coulombic efficiency of anodes [45, 60, 61]. Moreover, constructing Li composites, artificial SEI layer, and additives in the electrolyte is also adopted to stabilize the Li metal anode [62–64]. Finally, since the composition and formulation of the electrolyte are crucial for achieving stable and high-performance LSBs, a variety of liquid and solid electrolytes have been explored, with a focus on optimizing parameters such as ionic conductivity, electrochemical stability, and compatibility with cathode and anode [65–67].

Therefore, LSBs have made long-term strides in the performance from the rational design and modifications of cathode, anode, and separator to the electrolyte optimization tactics. However, the electrode–electrolyte interface is hard to be neglected as the energy exchange position of the LSBs. The interfacial physicochemical properties and stability are closely linked to the comprehensive performance [65, 68]. Recent research has focused on understanding the interface behavior to acquire a profound insight into the electrochemistry in LSBs. It is clearly shown in Fig. 1b that the issues in the cathode–electrolyte interface are strongly associated with its structure as well as the dissolution and diffusion of LiPSs. Thus, it is essential to understand the mechanisms underlying the challenges at the cathode–electrolyte interface, as feasible and affordable strategies are urgently needed to fuel the further development of LSBs [69, 70].

In this review, we will take a deep look at the bottleneck challenges and the corresponding optimization strategies at the cathode–electrolyte interface of LSBs. The critical challenges are discussed from structural and shuttle effect, respectively. Various methods are proposed to regulate the formation of cathode–electrolyte interphase (CEI) layer and the deposition pattern of Li_2S in order to enhance the structural stability. Moreover, comprehensive research is conducted to relieve the shuttle effect by restraining the LiPSs at the interface from three different reaction pathways. The limitations and possible future direction in manipulating the conductive and thermodynamically stable cathode–electrolyte interface to improve the durability of LSBs are also claimed.

2 Challenges of Cathode–Electrolyte Interface

It is crucial to explore the origin of the challenges at the cathode–electrolyte interface before employing the strategies. It stems not only from the formation of the CEI layer but also from the conversion mechanism mentioned above. The CEI layer is generally formed at the interface during the first cycling. The deposition of Li_2S and shuttle effect also takes place at the cathode–electrolyte interface. During cycling, the fracture of the CEI layer and uneven deposition of the Li_2S take a heavy toll on the interface stability. The shuttle effect triggered by the dissolution of LiPSs at the interface requires urgent care for the high-power LSBs.

2.1 Interface Structural Changes

2.1.1 Fractured CEI Layer

The CEI layer serves as a protective barrier at the cathode–electrolyte interface to safeguard the entire cathode and prevent direct contact between LiPSs and electrolyte [77, 78]. Understanding its formation mechanism and factors leading to instability of the CEI layer is crucial for enhancing the cathode–electrolyte interface. It is widely accepted that the formation of the CEI layer is closely associated with the deposition of electrolyte and oxidation of solvent molecules on the active cathode surface [79–83].

In the case of LSBs, the formation mechanism of the CEI layer varies across different electrolytes (Fig. 3a) [84–86]. For instance, in a carbonate-based electrolyte system consisting of 1.0 M $LiPF_6$ in ethylene carbonate (EC)/ethyl methyl carbonate (EMC) (3:7 by wt%) with 2 wt% vinylene carbonate (VC), the CEI layer is generated through the nucleophilic reaction between the C–O/C=O bonds and Li_2S_2, resulting in

https://doi.org/10.1007/s40820-024-01573-4

the formation of LPF-carbonate with C–S bonds and inducing further solvent decomposition. The primary components of the CEI layer are organic compounds. On the other hand, in an ether-based electrolyte containing lithium bis(fluorosulfonyl) imide (LiFSI), 1,2-dimethoxyethane (DME), 1,1,2,2-tetrafluoroethyl-2,2,3,3-tetrafluoropropyl ether (TTE) at the molar ratio of 1:1.2:3, DME solvent is hard to degrade because of the connect between its abundant C–O bonds and Li^+. In contrast, the LiF is formed due to the high activity of Li_2S_2 to C–F bonds in TTE giving rise to the decomposition of the TTE. Moreover, the reaction between the LiFSI and Li_2S_2 will break the S–N bonds and generate SO_x-F species. Thus, the CEI layer is dominated by the SO_x-F species and the limited LiF in the ether-based electrolyte.

Actually, systematically understanding the formation, structure, composition as well as the tailored interphase chemistry of CEI layers, remains an ongoing research. The formation of the stable CEI layer in common electrolytes also poses challenges. In common ether electrolytes, the high solubility of LiPSs inhibits the formation of a solid-state CEI layer. Additionally, the continuity and densification of the CEI layer are negatively impacted by low-activity lithium salts like trifluoromethanesulfonimide (LiTFSI). Although the carbonates can facilitate the formation of a relatively dense CEI layer in common carbonate systems (e.g., EC:EMC = 1:2 with 1 M LiTFSI), the uninterrupted direct contact between carbonates and LiPSs allows for continuous reactions between LiPSs and C=O groups of the ester electrolyte, resulting in a poorly controlled thickness of the CEI layer, which may eventually lead to passivation of the cathode–electrolyte interface [87, 88]. Furthermore, the porosity of S host and S content also influences the formation and stability of the CEI layer. Excessive porosity of the host material and excessively small particles of the S may hinder the formation of a closed CEI layer (Fig. 3b) [89]. When the S content is too high, the formed CEI layer may fracture due to the inability to withstand mechanical stress, owing to the difference in density between S and Li_2S (Fig. 3c) [90].

2.1.2 Uneven Li_2S Deposition

The deposition of the insulating product Li_2S at the cathode–electrolyte interface is generally thought to be the rate-determining stage during the discharge process of LSBs. It is necessary to explore its mechanism before taking further action to improve the reaction kinetics of the LSBs. The deposition of Li_2S is commonly presented as a nucleation–proliferation–growth model (Fig. 4a) [91].

Firstly, the Li_2S nucleates on the cathode substrate by overcoming a high interfacial impedance [92]. As-formed nucleates typically precipitate as islands after merging with LiPSs at the cathode–electrolyte interface driven by an electrochemical process, where the impedance between similar species is rather low [93]. Subsequently, the insulating Li_2S islands will keep expanding and eventually proliferate into a layer at the interface, which will hinder the electron transfer at the S host interface, passivating the cathode and decreasing S utilization [94]. As vividly shown in Fig. 4b**,** the conventional 2D growth will lead to the uneven deposition pattern of insulating Li_2S [95]. However, the Li_2S can continuously come into formation with limited electrons though unevenly deposited. The underlying reasons could be diverse. It has been proposed that Li_2S_4 can disproportionately form Li_2S_7 and Li_2S in the absence of electrons [96, 97]. There exists a possible reaction pathway whereby the Li_2S layer can persist in growing when the electrons can hardly transfer through the as-formed layer. This might further result in problems. Furthermore, it has been found that the morphology of the Li_2S is connected to the electrocatalytic characteristics of the deposition surface. At the electrocatalytic surface, the crystalline and spherical Li_2S is observed, while on a regular conductive surface, the amorphous and irregular Li_2S is deposited unevenly [98]. It is probably due to the limited electron access and part of the thick Li_2S layer could not be oxidized, thus leading to the uneven deposition of Li_2S, or what is known as "dead Li_2S" as shown in Fig. 4c. Essentially, such uneven Li_2S deposition on the cathode will function as an insulating layer and passivate the cathode–electrolyte interface. It can even block pores of the host and impede electrons/ions diffusion, leading to sluggish reaction kinetics, an increase in interfacial impedance, and rapid capacity decay. Meanwhile, the irregular Li_2S layer may also damage the structure of the cathode–electrolyte interface and influence the homogeneous reaction of the subsequent sites.

2.2 Shuttle Effect

The multi-step conversion of long-chain LiPSs generated at the cathode–electrolyte interface in the LSBs always results

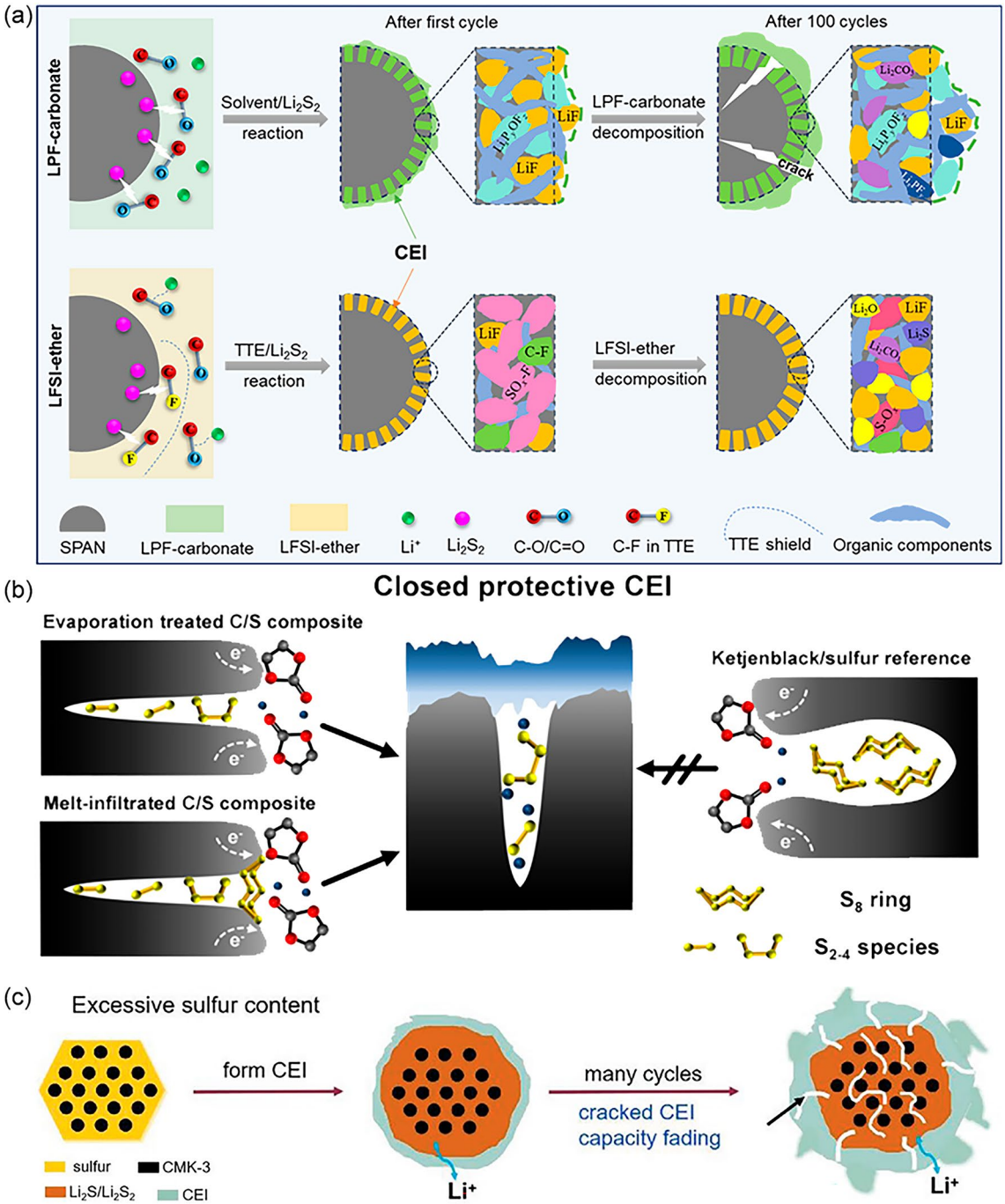

Fig. 3 **a** Diagram of CEI formation mechanism and process for SPAN in LPF-carbonate and LFSI-ether electrolytes. Reproduced with permission from Ref. [86], Copyright 2022, American Chemical Society. **b** Schematic illustration of the evaporation treated, melt-infiltrated composite, and Ketjenblack/S cathode during initial discharge process of CEI formation. Reproduced with permission from Ref. [89], Copyright 2020, John Wiley and Sons. **c** Schematic illumination of fractured CEI layer with an excessive S content. Reproduced with permission from Ref. [90], Copyright 2022, John Wiley and Sons

in more serious problems because of their severe solubility in most common ether-based electrolytes. The process of the shuttle effect can be divided into the following stages (Fig. 5a). (1) The solid S_8 is reduced to long-chain soluble LiPSs at the cathode–electrolyte interface. (2) The LiPSs detach from the S host and diffuse into the electrolyte. (3)

https://doi.org/10.1007/s40820-024-01573-4

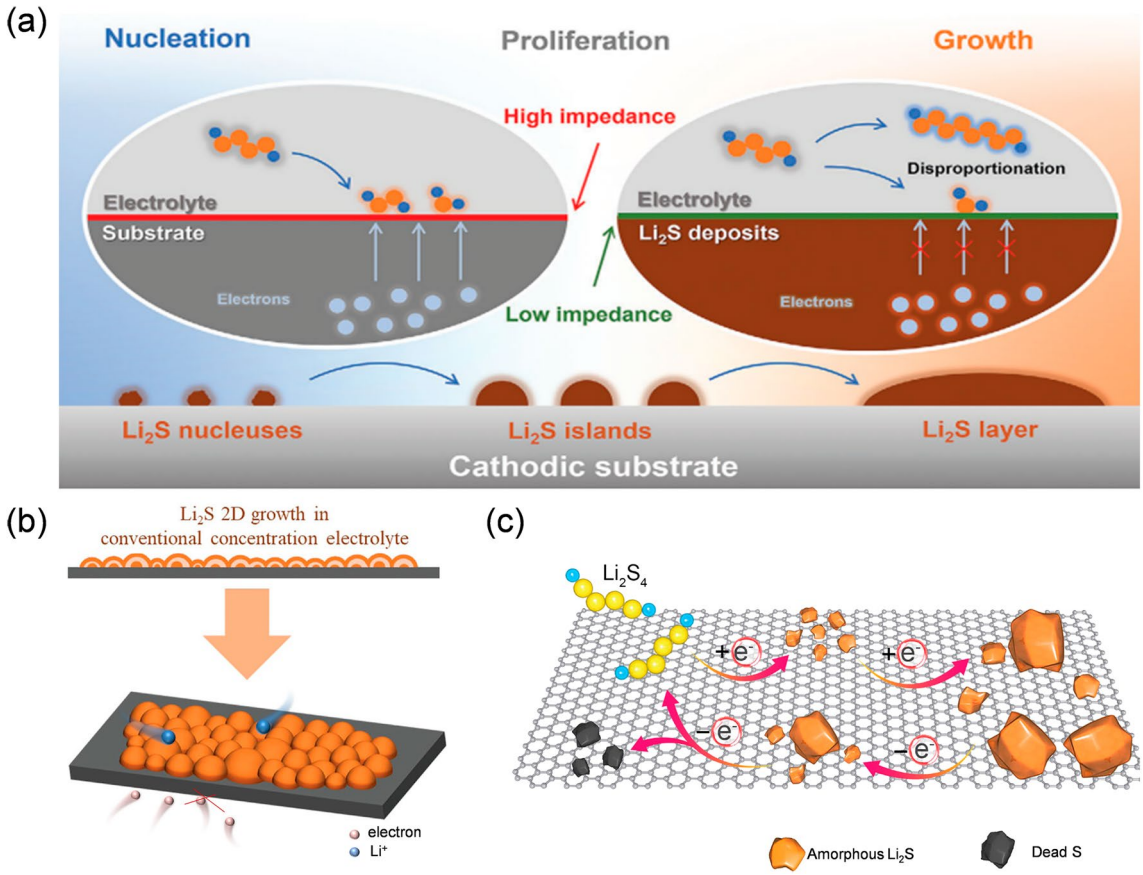

Fig. 4 **a** The "nucleation–proliferation–growth" model of Li_2S. Reproduced with permission from Ref. [91], Copyright 2023, John Wiley and Sons. **b** Illustration of Li_2S 2D growth. Reproduced with permission from Ref. [95], Copyright 2023, John Wiley and Sons. **c** Deposition of Li_2S on non-electrocatalytic surface. Reproduced with permission from Ref. [98], Copyright 2022, Elsevier

The dissolved LiPSs shuttle to the anode side and have side reactions with the lithium, leading to the partial loss of the active materials and impeding the reaction kinetics. (4) In the charging process, the LiPSs will shuttle back to the cathode under the action of electric field force and have a disproportionation reaction with S_8, to form soluble Li_2S_6 and Li_2S_8, which further intensifies the loss of the active materials and deteriorates the structure of the S cathode [99–101]. For instance, compared to the proper host NC@TiO_2-CNFs/S, other hosts like TiO_2-CNFs/S and Co/CoN-CNFs/S cannot inhibit the shuttle effect and this results in the woeful degradation of active S accompanied with irreversible capacity loss and extreme decrease in coulombic efficiency as illustrated in Fig. 5b, c, plaguing the wide-scale application of LSBs [102].

Understanding the origins of challenges at the cathode–electrolyte interface is of great importance. On the one hand, the fractured CEI layer due to the volume change of cathode and uneven deposition of Li_2S can damage the interface structure. On the other hand, the dissolution of long-chain LiPSs at the cathode–electrolyte interface will not only cause the constant loss of active materials from the S cathode but also cause the electrolyte to become more viscous. However, the systematic and more profound research on these thorny problems is worthy of more attention to provide a novel specific solution perspective.

3 Interface Tailoring Strategies

In order to address the aforementioned thorny issues of cathode–electrolyte interface to achieve efficient Li^+ diffusion kinetics for LSBs, significant strategies have been

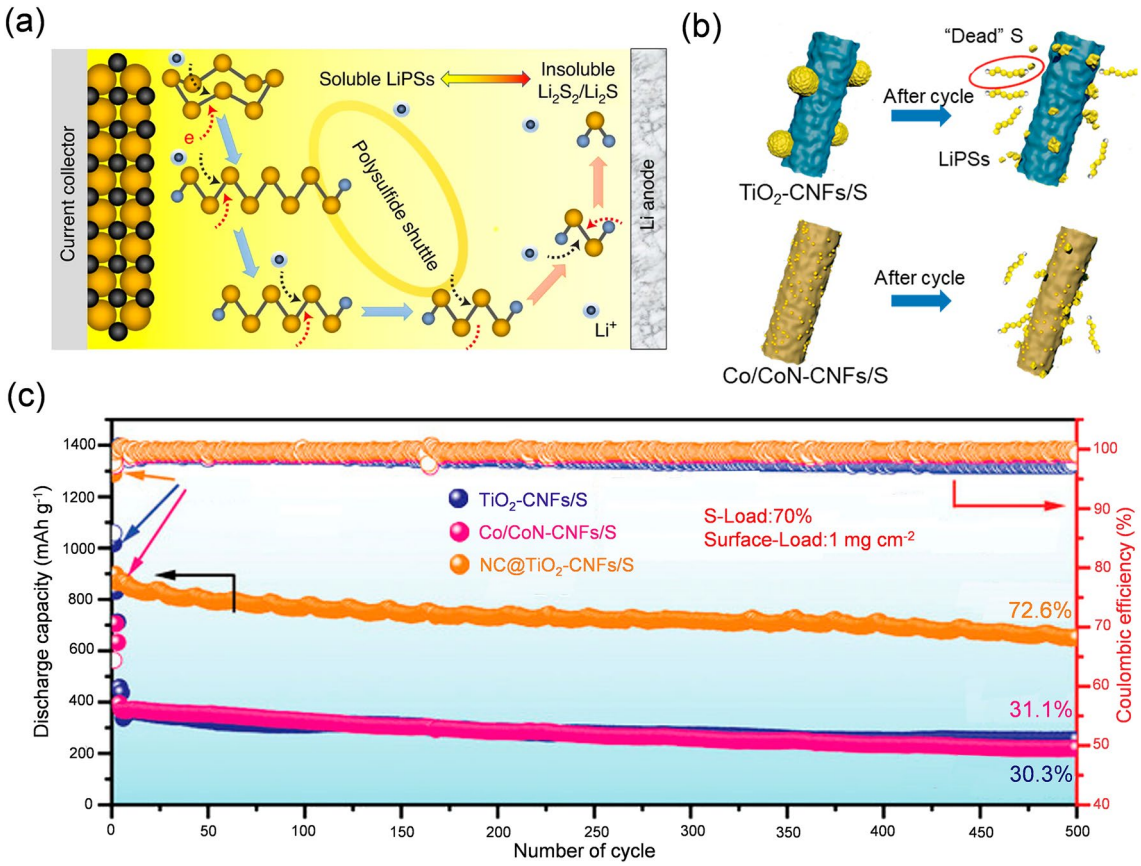

Fig. 5 **a** Schematic illustration of shuttle effect. Reproduced with permission from Ref. [99], Copyright 2020, Springer Nature. **b** Schematic illustration of examples of improper hosts like TiO_2-carbon nanofibers (CNFs)/S and Co/CoN-CNFs/S causing shuttle effect. **c** Cycling performance with TiO_2-CNFs/S, Co/CoN-CNFs/S, and NC@TiO_2-CNFs/S as host, respectively. **b, c** Reproduced with permission from Ref. [102], Copyright 2023, John Wiley and Sons

developed for tailoring the interface structure and suppressing the shuttle effect.

3.1 Interface Structural Tailoring

3.1.1 Structural Enhancement of CEI Layer

The development of the CEI layer is closely linked to the cathode and the electrolyte. To ensure a uniform and dense CEI layer, it is crucial to manage cathode volume expansion and optimize the electrolyte composition [103].

Previous studies have demonstrated that the CEI layer rupture caused by cathode volume expansion could be restrained by applying a suitable matrix host. Nanocarbon materials possessing abundant pores and good flexibility are typically exploited to load S. For instance, graphene matrix can effectively mitigate the S volume expansion because its many inner gaps could guide S lithiation along its open ends (Fig. 6a) [43]. Li et al. designed a molybdenum carbide decorated N-doped carbon hierarchical double-shelled hollow spheres (N–C HDS-HSs) electrode [104]. A buffer space for S expansion was provided by the double-shell hollow structure, while the thick mesoporous inner shell and central voids significantly increased the loading content of S. Thus, the electrode performed an ultra-high cycling stability with a capacity of 1075.1 mAh g^{-1} and a retention rate of 96.3% after 100 cycles at 0.2 C. Chen et al. found that the CEI layer was intolerant to the volume change and fractured during repeated lithiation/de-lithiation when the volume of the reduction product (Li_2S/Li_2S_2) surpassed the maximum volume of the host [90]. When the discharge becomes deeper, moreover, the volume expansion of Li_2S increases and probably causes the instability and cracking of the CEI layer. Therefore, adjusting the depth of discharge by

 https://doi.org/10.1007/s40820-024-01573-4

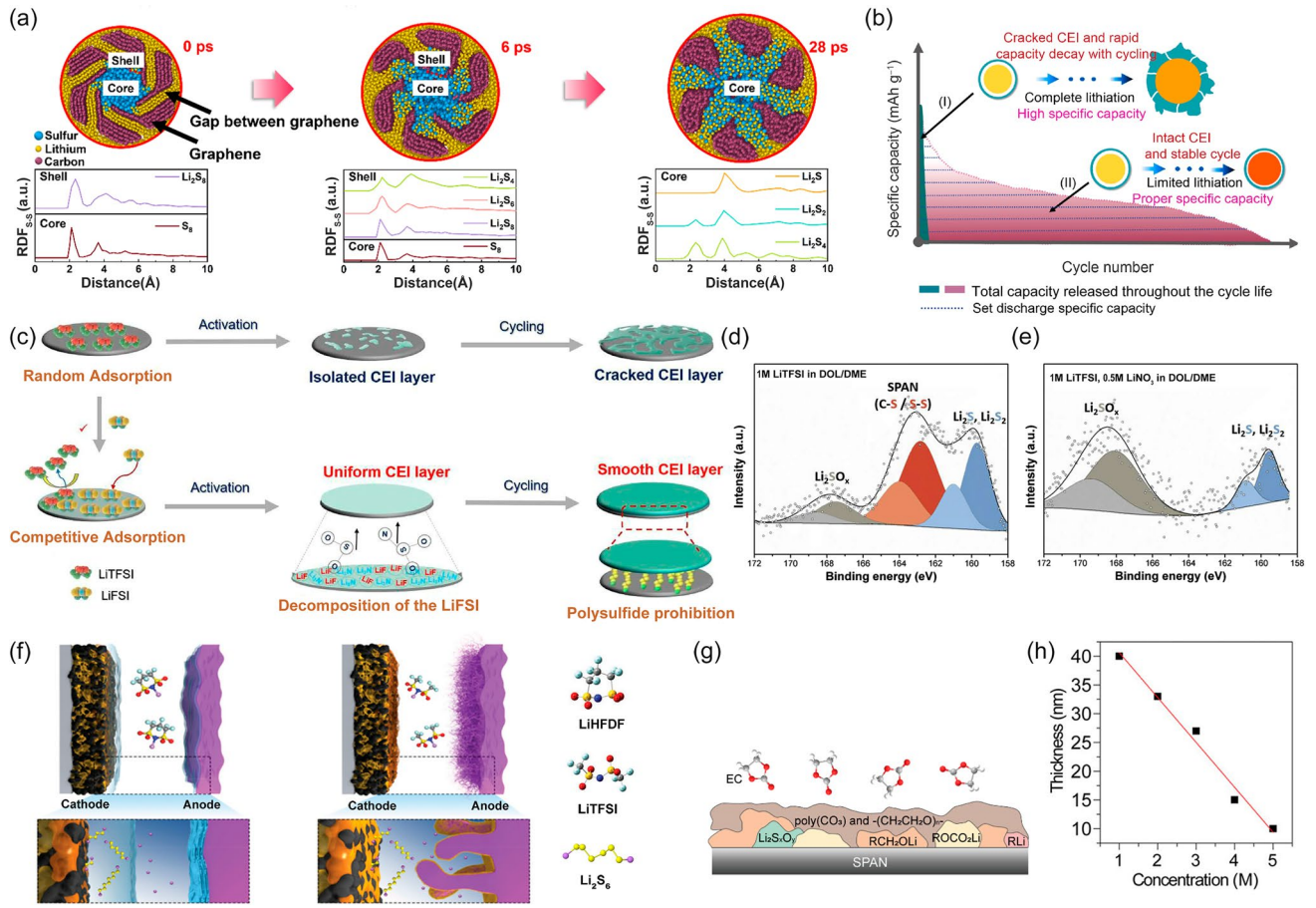

Fig. 6 **a** Lithiation of the S with graphene hosts and RDFs of S–S atom pairs of lithiation of the S with graphene hosts at different times. Reproduced with permission from Ref. [43], Copyright 2024, Elsevier. **b** Schematic illustration of the fundamental functions of capacity control on the cycle life evolution of cells. Reproduced with permission from Ref. [106], Copyright 2022, Elsevier. **c** $TFSI^-$ and FSI^- anion on FeS_2@3DNPC electrodes. Reproduced with permission from Ref. [112], Copyright 2022, Elsevier. XPS S 2*p* spectra of polyacrylonitrile (SPAN) cathode cycled in **d** 1 M LiTFSI and **e** 1 M LiTFSI-0.5 M $LiNO_3$ in 1,3-dioxolane (DOL)/1,2-dimethoxyethane (DME). **d**, **e** Reproduced with permission from Ref. [109], Copyright 2019, Elsevier. **f** The schematic illustration of how LiHFDF suppresses dissolution/shuttling of LSBs. Reproduced with permission from Ref. [113], Copyright 2020, John Wiley and Sons. **g** Schematic structure component of CEI layer formed in 1 M LiFSI/DME-EC. Reproduced with permission from Ref. [114], Copyright 2021, American Chemical Society. **h** The relationship between the thickness of the CEI layer and LiTFSI concentration. Reproduced with permission from Ref. [115], Copyright 2023, John Wiley and Sons

rationally managing the battery capacity and other discharge conditions is another effective way to safeguard the CEI layer (Fig. 6b) [105, 106]. One work reported that when the discharge specific capacity was limited to 300 mAh g^{-1} per cycle, the battery with an S loading of 4.56 mg cm^{-2} maintained a stable CEI layer and had a cycle life of more than 950 cycles with a capacity of 289 Ah g^{-1} over the course of its entire life.

Lithium salts, as the cornerstones of electrolytes, play a pivotal role in the formation of the CEI layer. As the commonly used lithium salt, the breakdown of anionic $TFSI^-$ allows a certain quantity of LiTFSI molecules to be uniformly and smoothly attached to the cathode surface, forming a CEI layer rich in LiF^-. With a high mechanical strength and ability to withstand the electrode volume change, the inorganic-rich CEI layer improves the electrochemical stability and suppresses irreversible reactions of electrolyte [107, 108]. Yet, a dense and continuous CEI layer is hardly obtained by utilizing LiTFSI alone due to the low activity of $TFSI^-$ (Fig. 6c). It is impressive how adding co-salts can alleviate this problem. Concentrated ether-based electrolytes containing LiTFSI and $LiNO_3$ can promote the formation of a CEI layer consisting of LiF and $LiNO_2$ [109]. Meanwhile, the detection of the Li_2SO_x component in the CEI layer demonstrated that the Li_2S/Li_2S_2 was oxidized by $LiNO_3$ (Fig. 6d, e). Li_2SO_x has a stronger conductivity

than Li_2S/Li_2S_2 and contributes to constructing a sturdy solid-state CEI layer, which minimizes the direct exposure of discharge products to the electrolyte and so limits the generation and dissolution of soluble LiPSs. Also, the decreasing Li_2S/Li_2S_2 on the cathode surface sharply decreases the cathode passivation. Previous studies have shown that LiFSI salt is unfavorable to LSBs over extended cycles because it has a high activity to react with LiPSs irreversibly, leading to S depletion [110]. However, it has been found recently that rational utilization of its high activity is beneficial for the formation of dense CEI layers containing large amounts of LiF-Li_3N (Fig. 6c) [111, 112]. Additionally, reducing solvent adsorption on the cathode surface, lowering the Li^+ desolvation barrier, and generating more free Li^+ ions for fast transition kinetics were all made possible by the CEI layer, which provided an exceptional performance for LSBs. Satisfactory effects were also demonstrated by other highly active lithium salts with comparable decomposition components. The use of lithium 1,1,2,2,3,3-hexafluoropropane-1,3-disulfonimide (LiHFDF) results in a persistent physical barrier made up of LiF and Li_3N by its cyclic and highly fluorinated anions construct, which confines LiPSs in the cathode bulk (Fig. 6f) [113]. With the S loading is 8.36 mg cm^{-2}, the battery performed an initial area capacity of 7.49 mAh cm^{-2} (≈ 896 mAh g^{-1}) and the capacity drops to 3.86 mAh cm^{-2} after 110 cycles. In the LiTFSI electrolyte, in contrast, the area capacity rapidly decreased to 1.5 mAh cm^{-2} after only 40 cycles from initial 7.65 mAh cm^{-2} (≈ 811 mAh g^{-1}) with a S loading of 9.43 mg cm^{-2}.

Dynamic regulation of the CEI layer through electrolyte modification is another effective initiative to preserve a stable cathode–electrolyte interface. A conformal polycarbonate-CEI layer, for example, can be induced at the interface when ethylene carbonate (EC) is designed as a co-solvent in ether electrolyte [114]. This layer is dominated by the organic (i.e., poly(CO_3) and $-(CH_2CH_2O)_n-$) (Fig. 6g). The increase in organic composition in a dense CEI layer enables to eliminate the LiPSs leakage and alleviate the electrolyte decomposition over time, thus achieving the thickness self-control. Also, the continuous presence of EC components in the electrolyte enables the repair of the highly variable CEI layer and keeps it dense. Additionally, the electrolyte modification notably facilitates the favorable role of LiTFSI for the formation of the CEI layer. Chang et al. further demonstrated that the $TFSI^-$ was critical for the formation of a thin and dense CEI layer when VC served as the solvent [115]. As depicted in Fig. 6h, the thickness of the CEI layer varied with varying $TFSI^-$ concentrations, most likely as a result of direct changes in the solvation structure and solvent activity of Li^+ caused by the concentration of LiTFSI in electrolytes. Stated differently, $TFSI^-$ may quantitatively regulate the structure of the CEI layer by controlling the electrolyte concentration.

3.1.2 Deposition Improvement of Li_2S

Li_2S tends to grow uncontrollably on the cathode surface as an insulating product in LSBs during the discharge process, which affects the conversion of LiPSs by passivating the cathode surface and hindering the transfer of electrons/ions. Therefore, Li_2S deposition has to be improved. Generally, there are two means to that end. One is to achieve high Li_2S solubility, and the other is to induce Li_2S uniform deposition.

Strong interaction between the N–H bond and S^{2-} anion can access high Li_2S solubility. The high electropositivity of the H atom in the N–H bond in ammonium salt, like NH_4TFSI, can serve as a hydrogen bond donor to form H–S bonds with S^{2-}, which in turn facilitates the dissociation of Li_2S [116]. Since NH_4TSFI promotes the high solubility of Li_2S through the solvation process, its addition to the electrolyte can significantly reduce particle aggregation on the surface of the S/carbon tubes (CNT) cathode. In contrast with Li_2S, the binding energy of soluble S^{2-} substance can be electrostatically stabilized by Li^+, thereby facilitating the electrochemical S redox reaction. A similar behavior was also noted once the trifluoromethane sulfonamide (TFMSA) was added to the electrolyte, in which the S^{2-} in Li_2S and the amide hydrogen (N–H) engaged in strong interactions to form the H–S bonds (Fig. 7a) [117]. The dissolution of Li_2S at the interface produced more reaction sites for LiPSs conversion, accelerated the reaction kinetics, and raised the efficiency of the active S even with 1% TFMSA addition (Fig. 7b). Another approach for Li_2S dissolution is the Lewis acid–base principle. Owing to the stronger Lewis basicity of Li_2S compared to LiPSs, the solubilization of Li_2S is facilitated by sulfolane (SL) as a Lewis acid, which is capable of strongly interacting with Li_2S (Fig. 7c) [118]. As shown in Fig. 7d, the corresponding peak of Li_2S drops dramatically (161.8 eV) with the increase in SL content in the electrolyte. At S loading of 1.0 mg cm^{-2}, the cells containing 6% and

 https://doi.org/10.1007/s40820-024-01573-4

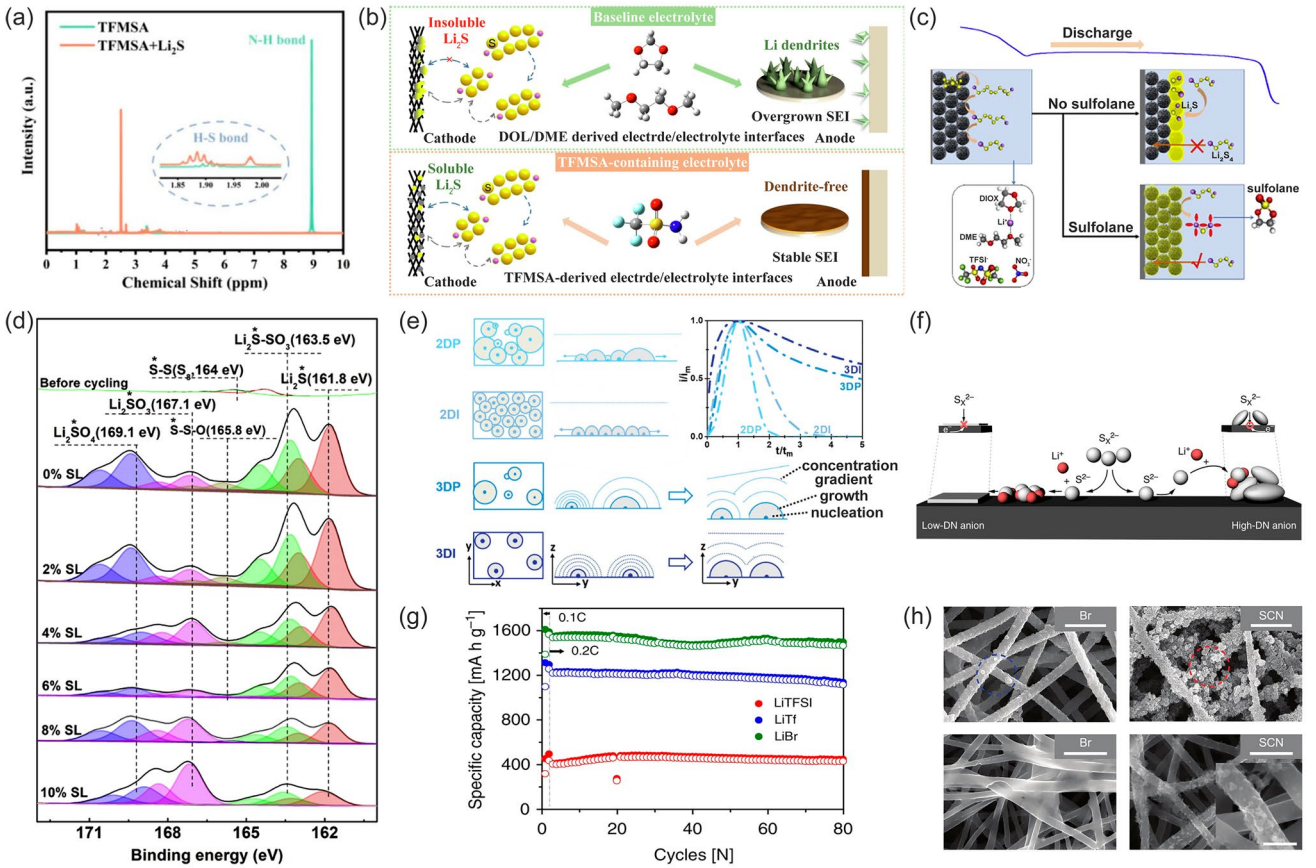

Fig. 7 **a** Hydrogen NMR spectra of TFMSA and TFMSA + Li_2S. **b** Positive effects of the TFMSA additive at electrode–electrolyte interfaces in the LSBs. **a**, **b** Reproduced with permission from Ref. [117], Copyright 2022, Elsevier. **c** Schematic diagram of enhancement effect of SL adding. **d** High-resolution S 2*p* XPS spectra of cathode surface with SL in 1 M LiTFSI in DOL/DME with 0.2 M $LiNO_3$ containing different content of SL. **c**, **d** Reproduced with permission from Ref. [118], Copyright 2020, Elsevier. **e** Schematic illustration of 2D progressive nucleation (2DP)/2D instantaneous (2DI) (BFT models) and 3D progressive (3DP)/3D instantaneous (3DI) (SH models) (*x*–*y* is parallel to the substrate; *y*–*z* is vertical to the substrate). Reproduced with permission from Ref. [119], Copyright 2019, John Wiley and Sons. **f** Schematic diagram of 3D growth of Li_2S induced by high donor number (DN) anions. **g** Comparison of the charge and discharge capacities for 80 charge/discharge cycles at 0.2 C. The electrolyte consists of 0.2 M LiPSs, based on Li_2S_8 and 1 M lithium salt Li_X, X = $TFSI^-$, Tf^-, or Br^-/0.2 M $LiNO_3$/DOL: DME (1:1). **f**, **g** Reproduced with permission from Ref. [120], Copyright 2019, Springer Nature. **h** Li_2S deposition morphologies in the cathode for the LiTFSI, LiBr, and LiSCN electrolytes after discharge at 0.05 C and 0.4 C. Reproduced with permission from Ref. [121], Copyright 2023, John Wiley and Sons

10% SL in 1 M LiTFSI in DOL/DME with 0.2 M $LiNO_3$ displayed a promising capacity of 1130 mAh g^{-1} and 1050 mAh g^{-1}, respectively, which were higher than that of the cells without SL additive in the electrolyte (1020 mAh g^{-1}).

Li_2S deposition on the cathode electrode surface follows an electrochemical deposition model (Fig. 7e) [119]. Generally, 2D Li_2S deposition is a major obstacle to achieving high reversible capacity in the glyme-based LSBs as it leads to rapid loss of active electrode surface and low S utilization. Conversely, 3D deposition is capable of mediating the radial growth of Li_2S, circumventing 2D laminar deposition and thus delaying electrode surface passivation. An effective strategy to achieve 3D growth of Li_2S is electrolyte-based operation. It is well established that DN of solvent affects the deposition pattern of Li_2S on the cathode surface. The passivation caused by uncontrollable Li_2S and the 3D growth can be encouraged by high DN solvents. Chu et al. designed electrolytes with high DN anionic lithium salts, such as lithium triflate (LiTf) and LiBr [120] Tf^- and Br^- have both potent solvation effects on Li^+ compounds, which can dissociate S^{2-} and increase the solubility of Li_2S on the cathode surface. When S^{2-} that has left the electrode surface combines with Li^+, Li_2S will be deposited on the top surface nearby agglomerates due to its high polarity and

then form a 3D structure (Fig. 7f). It significantly suppresses cathode interface passivation, prolongs the lower voltage plateau, and increases the discharge capacity to almost the theoretical value (Fig. 7g). Similar results are obtained from a novel thiocyanate anion (SCN^-) salt with a high donor number (DN = 25.6 kcal mol^{-1}). The dissociation of Li_2S is facilitated not only by the strong coordination between SCN^- and Li^+ but also by the direct interaction between SCN^- and S^{2-} [121]. Meanwhile, the short-chain LiPSs could be stabilized by electron-accepting C atoms in SCN^-, providing more chemical pathways for Li_2S deposition than those in the Br^- (Fig. 7h).

In addition to electrolyte additives, metal-based materials have important applications in mediating the 3D deposition of Li_2S because they provide a large number of reaction sites and improve the kinetic transformation process of S-containing materials. Tian et al. synthesized a composite host material of discrete Mo_5N_6 nanoparticles immobilized on graphene (G@MNNP) [122]. Because of its high catalytic activity, the Mo_5N_6 nanoparticles acted as favorable nucleation sites and guided isolated growth of the Li_2S at the cathode-side interface (Fig. 8a). Isolated growth retarded the merging of neighboring Li_2S nucleus and promoted their isotropic growth, and then, the 3D Li_2S evolution was facilitated. As shown in Fig. 8b**,** solid deposits on G@MNNPs consisted of isolated Li_2S following 5000 s of constant potential discharge. In contrast, the solid products on Mo_5N_6 nanolayer-coated graphene (G@MNNL) have relatively smooth morphology, indicating that Li_2S almost entirely coverage the surface. A similar result was seen in the SnO_2 nanodot (SND) modified Mo_2N microstrip [123]. In comparison with the bare Mo_2N, the SND/Mo_2N heterointerface prevented the surface passivation of the Mo_2N microstrip by facilitating the LiPSs adsorption and directing the 3D porous growth of Li_2S (Fig. 8c). The battery reached a capacity as high as 738.3 mAh g^{-1} after 550 cycles at 0.5 C, and its decay rate was only 0.025% per cycle (Fig. 8d).

It should be noted that the insulating Li_2S covering the catalytic site's surface will diminish the catalytic activity, which in turn impacts the deposition efficiency. Single-atom copper modified SA-Cu@NCNF can effectively resolve this issue as a host material [124]. SA-Cu draws effective charge "acceptance–donation" between Cu and S due to strong metal-substrate interactions, enabling Li_2S molecules to exhibit metal abundance with enhanced electronic conductivity (Fig. 8e). Assisted by the conducting Li_2S clusters, the SA-Cu sites covered by Li_2S clusters still serve as active sites for electrochemical reactions to further catalyze the 3D deposition of Li_2S (Fig. 8f). Consequently, the SA-Cu@NCNF/S electrode exhibited a decay rate of 0.038% per cycle at 5 C after 500 cycles. One more effective tactic is to use soluble redox mediators. As an exogenous redox mediator formed by on-surface electroreduction, $CoCp_2$ diffuses to the outer surface of pre-existing Li_2S nuclei at the electrolyte/conducting substrate/Li_2S triple-phase boundary and mediates Li_2S growth (Fig. 8g) [125]. The $CoCp_2$ always remained soluble during the catalytic process preventing changes in the amount and concentration caused by Li_2S deposition, which continuously maintained the 3D Li_2S growth. The discharge capacity of LSBs enhanced at least 8.1 times under harsh conditions like high multiplicity (> 1 C) or low electrolyte operation (electrolyte/S ratio of 4.7 uL mg^{-1}).

Additives featuring high dielectric constant, high viscosity, and appropriate DN are bound to improve the interface passivation due to the uneven deposition of Li_2S and can construct a dense, uniform, and stable interface with high activity. However, they might impede the lithium anode from being stable. In comparison, Metal-based materials are promising in favor of rapid 3D Li_2S deposition due to their interfacial synergistic catalytic and electronic modulation effects.

3.2 Shuttle Effect

The shuttle effect originating from the dissolution of LiPSs at the cathode–electrolyte interface leads to the loss of active materials and rapid capacity decay. Capturing LiPSs is the most popular method in the solid–liquid–solid stepwise reaction pathway among the explored strategies to lessen the severe shuttle effect of LSBs. Regulating the reaction pathway to limit the contact between the electrolyte and LiPSs is paid more and more attention. Herein, we will review the most recent advances in the perspective of diverse reaction patterns to mitigate the shuttle effect.

3.2.1 Adsorption of LiPSs in the Solid–Liquid–Solid Pathway

In the traditional solid–liquid–solid pathway, it is common to use diverse materials as the S host to absorb the LiPSs to

 https://doi.org/10.1007/s40820-024-01573-4

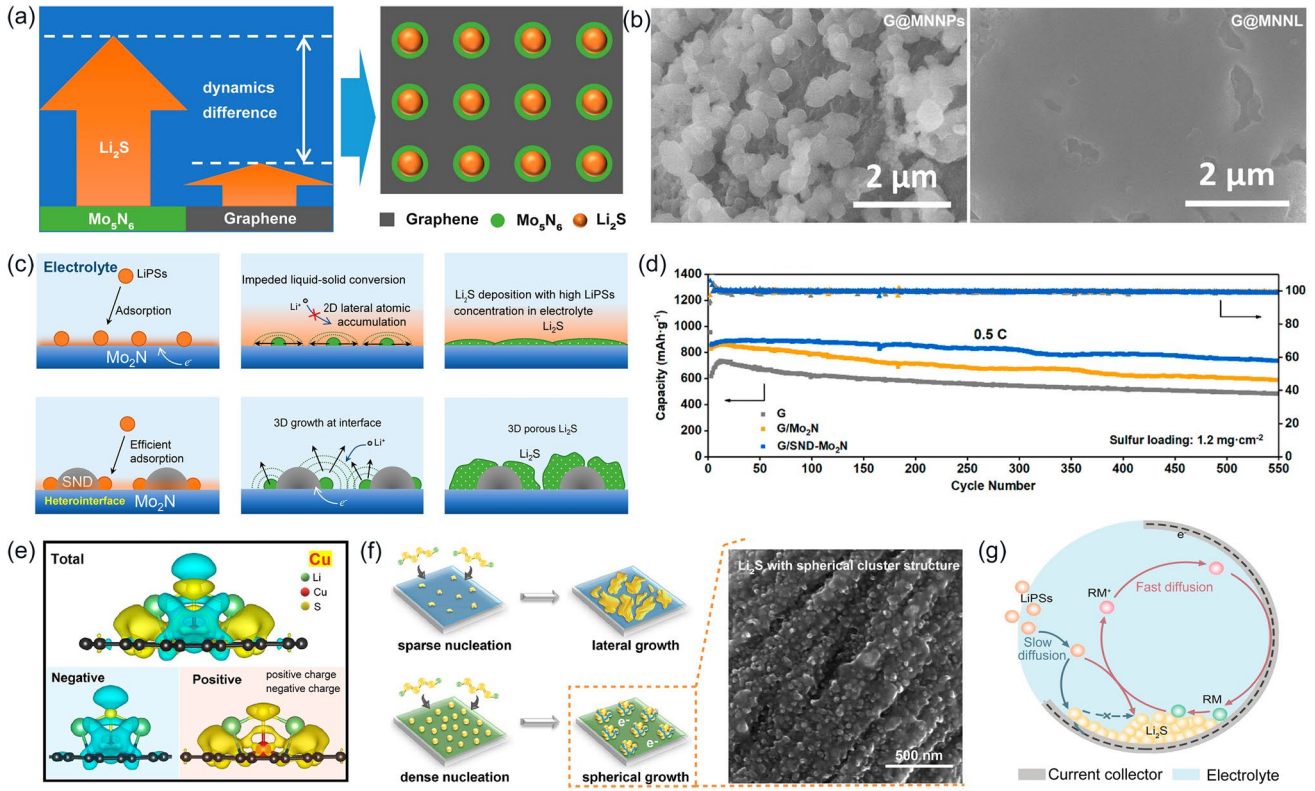

Fig. 8 **a** Schematic illustration of the nucleation behavior of Li_2S on G@MNNPs and **b** SEM images of G@MNNPs and G@MNNL after potentiostatic 5000 s discharge. **a**, **b** Reproduced with permission from Ref. [122], Copyright 2021, John Wiley and Sons. **c** Schematic conversions from LiPSs to Li_2S on the Mo_2N and SND-Mo_2N surfaces, respectively, and **d** their long-term cyclability for 550 cycles at 0.5 C. **c**, **d** Reproduced with permission from Ref. [123], Copyright 2021, American Chemical Society. **e** Charge density difference of SA-Cu@N-doped graphene (NG)/Li_2S. **f** Schematic illustrations of Li_2S deposition process on CNF (top) and N-doped carbon fiber foam (SA-Cu@NCNF) (bottom) substrates. **e**, **f** Reproduced with permission from Ref. [124], Copyright 2022, Elsevier. **g** Schematic illustration of the growing pathway of Li_2S in the absence (blue arrows) and presence (red arrows) of cobaltocene ($CoCp_2$). Reproduced with permission from Ref. [125], Copyright 2019, John Wiley and Sons

prevent shuttling in various ways. To date, functional carbon materials, polar metal compounds, polymers, and MXenes have been all widely applied for interfacial modification in the hope of achieving physical/chemical adsorption of LiPSs at the cathode–interface interface.

(1) Functional carbon materials

Functional carbon materials have gained extensive popularity in enhancing the energy storage performance of LSBs due to their unique physicochemical properties that benefit from distinct functional groups. Taking the N-doped carbon (NC) as an example, the N atoms are well known to be point defects and can significantly increase the carbon's overall conductivity and polarity. This enhancement makes it possible to bond LiPSs and confine the shuttle effect at the cathode–cathode–electrolyte interface [126]. Additionally, the interconnected NC increases the electric contact at the interface and improves the performance with a promising initial discharge capacity [127]. When the NC is further composited with transition metal compounds such as FeS (Fig. 9a, b) [128] and CeO_2 [129], the exposure of high active sites at the interface can be dramatically increased. This not only protects the cathode from depletion in electrolytes but also promotes redox reactions and enhances chemical adsorption of LiPSs through interaction with N atoms, thereby improving the overall conversion efficiency. Moreover, uniform depositing of the product Li_2S at the cathode-side interface can be observed upon additional cycling, meaning a significant advance in desired capacity and long-term cycling stability. When carbon is co-doped with N and O, the surrounding electronic structure of O atoms can be greatly adjusted, strengthening the bond between S and O by enhancing the chemical interaction [126]. As shown in

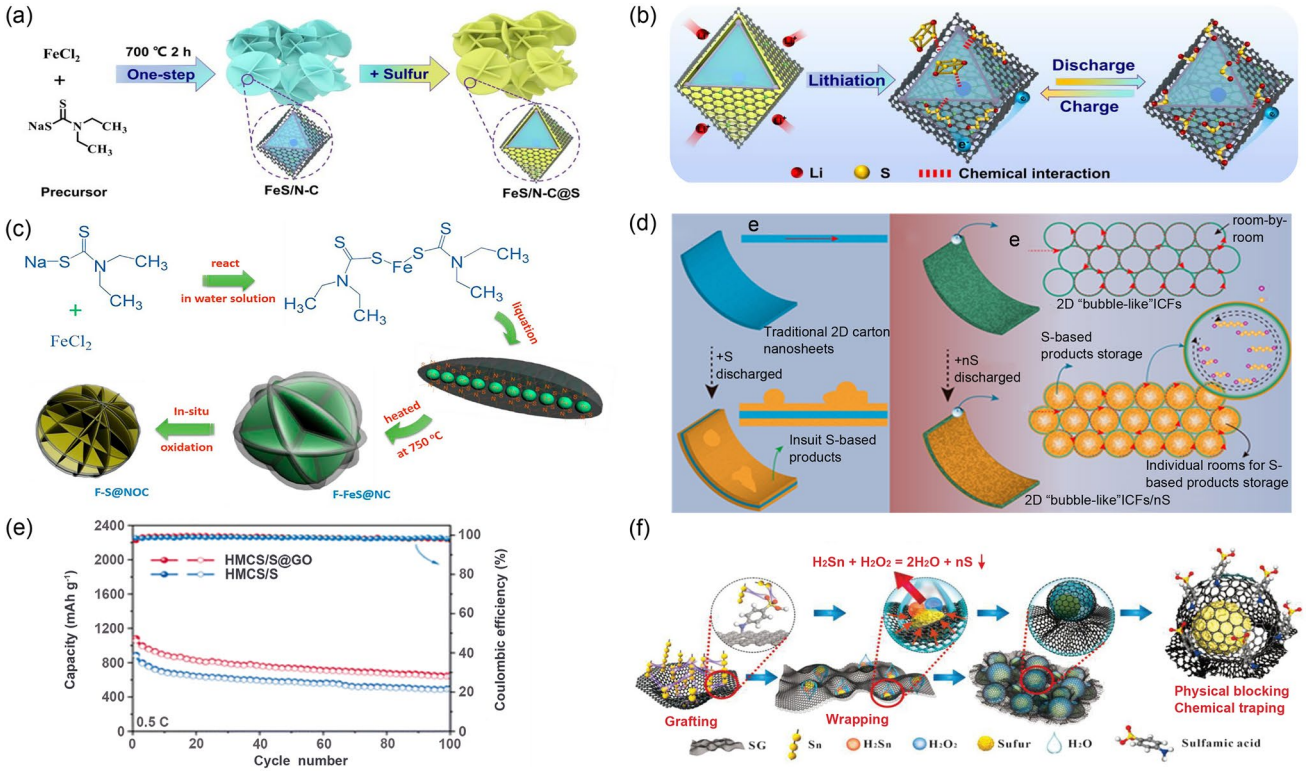

Fig. 9 The schematic of **a** synthesis procedure and **b** strong interaction with LiPSs during the charge/discharge process of FeS/N–C@S nanocomposite cathode. **a**, **b** Reproduced with permission from Ref. [128], Copyright 2021, Elsevier. **c** Schematic preparation of F-S@NOC composite. Reproduced with permission from Ref. [130], Copyright 2018, Elsevier. **d** Schematic comparison between the traditional 2D carbon/S and bubble-like ICFs/nS cathodes. Reproduced with permission from Ref. [131], Copyright 2017, American Chemical Society. **e** Cycling performance comparison between the HMCS/S composite and HMCS/S@GO cathodes. Reproduced with permission from Ref. [132], Copyright 2022, Royal Society of Chemistry. **f** Self-caging mechanism for the growth of yolk-shell graphene@S particles. Reproduced with permission from Ref. [133], Copyright 2021, John Wiley and Sons

Fig. 9c, Wang et al. prepared a composite cathode of flower-like N/O co-doped carbon coated S (F-S@NOC). Benefiting from the exposure of more N/O functional polar groups, the cathode was able to anchor LiPSs, exhibiting excellent rate performance and cycling stability with a low decay rate of only 0.069% per cycle over 500 cycles at 1 C [130].

With sufficient oxygen-containing functional groups such as epoxy, carboxyl, and hydroxyl groups, graphene oxide (GO) is considered a highly effective polar material for adsorbing LiPSs. Wu et al. used GO wrapped interconnected carbon fabrics/S (ICFS) as the cathode and successfully sealed the open access of ICFs to anchor S (Fig. 9d) [131]. Thanks to the polar adsorption of GO and the enhanced conversion kinetics by electronically uneven polarized S, the specific energy capacity of the pouch cell reached up to 1.55 Ah@315.98 Wh Kg^{-1} at 0.1 C. However, GO fragments are prone to accumulate, which leads to a significant exposure decrease in active surface and a deterioration of performance. Therefore, 3D GO with straight mesoporous access is designed to wrap on the surface of hollow carbon spheres (HMCS@GO) by electrostatic adsorption and interfacial van der Waals interactions [132]. It anchors LiPSs effectively as the S host. When the hollow carbon shell and mesopores that facilitate the Li^+ diffusion is combined, the conversion of LiPSs is promoted. Therefore, the initial discharge capacity of 1054 mAh g^{-1} is delivered at 0.5 C with a capacity retention rate of 60.2% after 100 cycles (Fig. 9e). Sulfonated graphene (SG), as another functional carbon material, was applied by Yu et al. to encapsulate S particles inside the atomic shells, forming self-assembled nanocages that can polarize S_8 through sulfonate groups on its surface (Fig. 9f) [133]. SG and S_8 interact strongly during the reaction due to the strong electronic absorption. Therefore, the excellent nanocage stability, the tight wrapping on S, and

 https://doi.org/10.1007/s40820-024-01573-4

the superior chemisorption of the sulfonic groups on LiPSs together construct a stable cathode interface and realize the advanced electrochemical performance of LSBs.

Although functional carbon materials possess a distinct ability to anchor LiPSs and excellent ionic/electronic conductivity to accelerate the reaction kinetics on a large scale, combining desired functionality to increase energy density remains a challenge that requires comprehensive consideration of the physical and chemical properties of various components.

(2) Polymer-based materials

Polymer-based materials have good affinity to LiPSs due to their rich polar functional groups (C–N, C–S, C–O) and conjugated structures with alternating C–C and C=C bonds [134]. O, N, and S heteroatoms in polar functional groups can achieve considerable chemisorption to LiPSs. In addition, some of them pose excellent electric/ionic conductivity, such as polypyrrole (PPy) [134–136], polyaniline (PANI) [137], and poly(3,4-ethylene dioxythiophene) (PEDOT) [138]. The introduction of polymer-based materials will also reduce the dissolvation of the LiPSs at the cathode–electrolyte interface.

PPy exhibits an electronic conductivity of 2–100 S cm^{-1} due to its hydrophilic and interconnected five-membered pyrrole rings. The electronic feature and long-chain structure allow its strong interactions with LiPSs and promote the redox reaction of LSBs [139]. Geng et al. used a ~ 55-nm-thick PPy layer to cover the hollow metal–organic framework (MOF) [140], which showed a significantly improved electrochemical rate and cycling performance. Dong et al. also applied PPy to coat the hollow layered double Ni-Co hydroxide (Ni-Co LDH) (Fig. 10a) [141], not only enhancing the chemisorption of LiPSs and overall electronic conductivity but also increasing the surface reaction rate and electrocatalytic activity of the Ni-Co LDH, facilitating reversible conversion between LiPSs and Li_2S_2 [142, 143]. At a current density of 1 C, the initial discharge capacity was 907.2 mAh g^{-1} and maintained at 633.4 mAh g^{-1} after 500 cycles (Fig. 10b). Coupling conductive polymers with polar materials can directly avoid the LiPSs to contact with electrolyte. For example, both highly defective (amorphous) black-TiO_2 [136] and hollow 1 T-MoS_2 skeleton (Fig. 10c, d) [135] can catalyze the conversion and limit the LiPSs dissolution through a synergistic interaction with the PPy layer. Poly(3,4-ethylene dioxythiophene): poly(styrenesulfonate) (PEDOT:PSS) is also designed to form an interface layer on the spherical double-layered hollow C/S composite. This unique design enabled multiple components in the cathode to work well and showed outstanding cycling stability with a capacity decay rate of 0.097% during 500 cycles [144].

Polymer-based materials can also be used to modify the cathode–electrolyte interface on a cathode scale. Oxidative chemical vapor deposition (oCVD) is an emerging deposition process that generates conjugated polymer films by gas-phase reaction with high conductivity, excellent homogeneity, and conformal properties [146]. Zhang et al. deposited o-PEDOT on cathode using oCVD, which was able to fix the LiPSs through physical encapsulation and chemisorption, effectively limiting the dissolution of LiPSs in the electrolyte (Fig. 10e) [145]. Meanwhile, the o-PEDOT layer with a highly conductive network structure can provide more charge and mass transfer sites for insoluble LiPSs, facilitating the solid–solid conversion reaction kinetics. The S cathode with o-PEDOT in pouch cell provided an initial capacity of 732.8 mAh g^{-1} at the current density of 1.5 mA cm^{-2} with a high S loading of 11 mg cm^{-2}. It has a high discharge capacity of 567.1 mAh g^{-1} even after 50 cycles (Fig. 10f).

Polymers have been demonstrated to relieve the shuttle effect for enhancing the electrochemical performance of LSBs, but further efforts are needed to explore scalable and economically advantageous technologies. Meanwhile, controlling coating thickness to create a uniform cathode–electrolyte interface that maximizes performance is also a future task.

(3) Polar metal-based compounds

Generally, polar–polar interactions are stronger than polar–nonpolar interactions, and binding energy is one of the key factors in evaluating the dominance of adsorption ability [147]. Since LiPSs are polar compounds, the introduction of polar metal-based compounds can also adsorb the LiPSs through polar–polar interactions.

As shown in Fig. 11a, the binding energy for chemical adsorptions of the polar metal compounds (such as metal oxides and metal MOF center or non-stoichiometric metal center) is much higher than that of the normal physical adsorptions [148]. To enhance the reaction performance of cathode–electrolyte interface, polar metal compounds with rich polar active sites have captured wide attention in LSBs research. They exhibit more efficient adsorption to LiPSs via not only physical trapping but also through strong chemical bonds, such as the Li bond or S bond [149, 150]. With fruitful works completed, a variety of polar metal

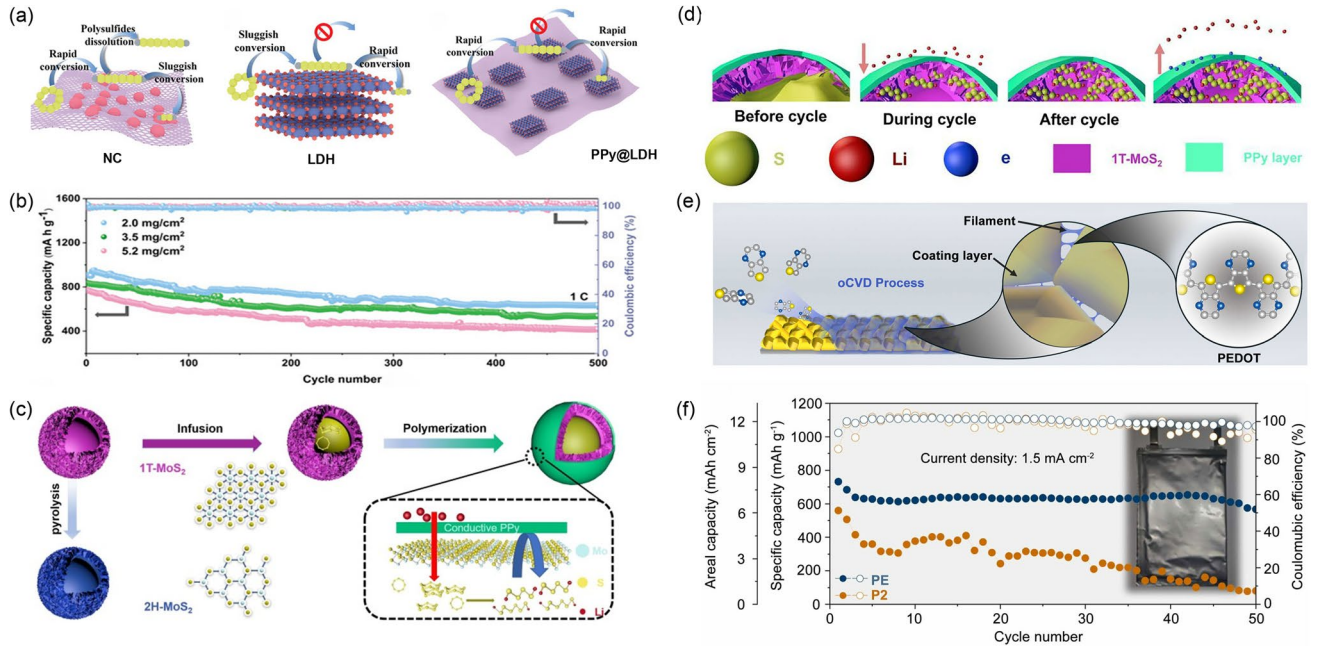

Fig. 10 **a** Schematic illustrations of S adsorption and catalyzation on NC, LDH, and PPy@LDH. **b** Long-term cycling performance of the PPy@LDH-S cathodes with different S loadings in cells. **a**, **b** Reproduced with permission from Ref. [141], Copyright 2023, John Wiley and Sons. **c** Schematic illustrations of synthesis and **d** LiPSs trapping mechanism of 1 T-MoS_2-S@PPy cathode. **c**, **d** Reproduced with permission from Ref. [135], Copyright 2022, Elsevier. **e** The fabrication process of o-PEDOT modified S cathode. **f** Cycling performances of Li–S pouch cells with the P2 and PE cathodes, respectively. **e**, **f** Reproduced with permission from Ref. [145], Copyright 2023, Elsevier

compounds, including oxides, sulfides, and nitrides, have been widely proposed as appropriate interface modification materials in LSBs [150]. Moreover, some transition metal oxides (WO_3 [151], CeO_2 [152], and MoS_2 [153]) show good catalytic properties and accelerated redox kinetics of the S conversion.

Yu et al. reported an effective way to alleviate the shuttling of LiPSs by coating TiO_2 on the NG/S composite cathode [154]. Due to TiO_2 acting as a Lewis acid and LiPSs acting as a Lewis base, electrons are transferred to NG/S to form Li-N and S-Ti bonds with LiPSs during the reaction. Therefore, the TiO_2-NG/S cathode maintains a high discharge capacity of 918.3 mAh g^{-1} after 500 cycles due to the strong binding energy of 3.59 eV (Fig. 11b). Kim et al. designed a novel polymeric cobalt (Pc) containing triethylene glycol linkers (TCP) to coat on multiple wall carbon nanotubes (MCs) through a strong π–π interaction and formed a polar TCP/MCs composite (Fig. 11c) [155]. The TCP creates a lipophilic environment for the uniform distribution of Li^+ active sites, thus accelerating Li^+ diffusion [156, 157]. The lithophilic triethylene glycol (TEG) could anchor Li^+ to the active site of LiPSs, and the Co atom will accept electrons from S atoms in Li_2S_6, subsequently forming a stable Co-S bond. Meanwhile, the N atoms in TCP and TEG linkers can form N-Li and O-Li bonds with the Li atoms in Li_2S_6, and the TCP layer also provides various Lewis acid–base binding sites for LiPSs, preventing the formation of insulative S composite species.

Both Yu et al. and Kim et al. developed different approaches to enhance the conversion of LiPSs by creating more favorable active sites for adsorption. It is worth noting that stronger binding energy is not always beneficial. When it exceeds 5 eV, LiPSs may be trapped at the cathode surface, hindering its conversion and causing secondary dissolution [158]. Polar metal compounds with moderate adsorption ability are preferred in LSBs. However, most metal oxides have poor electronic conductivity, leading to slow redox kinetics and inevitably impeding the direct LiPSs conversion at the interface [159].

(4) MXenes

As a class of 2D materials with polar characteristics, thermal stability, and manipulable Lewis acidic surface, MXenes are extensively used to modify the cathodes to confine the LiPSs shuttling of LSBs [160]. Compared to most polar

https://doi.org/10.1007/s40820-024-01573-4

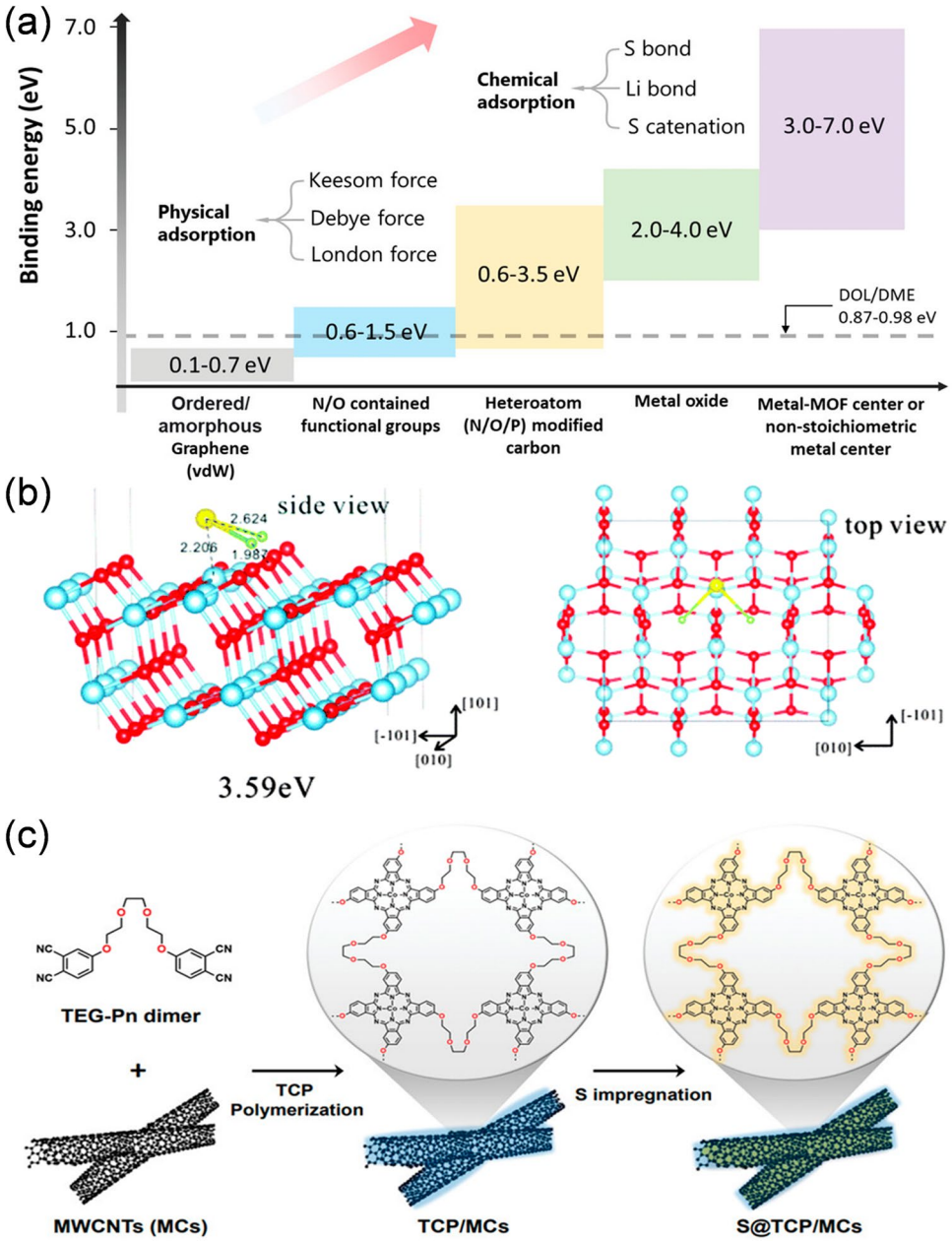

Fig. 11 **a** Binding energy scope of categorized adsorbents to LiPSs. Reproduced with permission from Ref. [148], Copyright 2022, John Wiley and Sons. **b** Adsorption configuration of Li_2S on anatase-TiO_2 (101) surface. Reproduced with permission from Ref. [154], Copyright 2016, Royal Society of Chemistry. **c** Schematic preparation of the S@TCP/MCs electrode. Reproduced with permission from Ref. [155], Copyright 2023, John Wiley and Sons

metal compounds, MXenes tend to have excellent conductivity to accelerate the interface reaction kinetics [161].

In a study by Wang et al. (Fig. 12a), three-dimensional S-CNT@MXene cages were reported, where ultrathin MXene nanosheets were utilized around S-CNT porous spheres [162]. The spherical structure avoids the restacking of MXene and makes full use of its active sites, improving the Li^+ diffusion at the interface. Due to the abundant terminal groups of -OH, -O, and -F on the MXene surface, the composite exhibits significant chemical adsorption with LiPSs and facilitates electrolyte penetration. The UV/Vis spectra showing a remarkable blueshift of the absorption edge further confirmed the strong chemical interaction between CNT@MXene

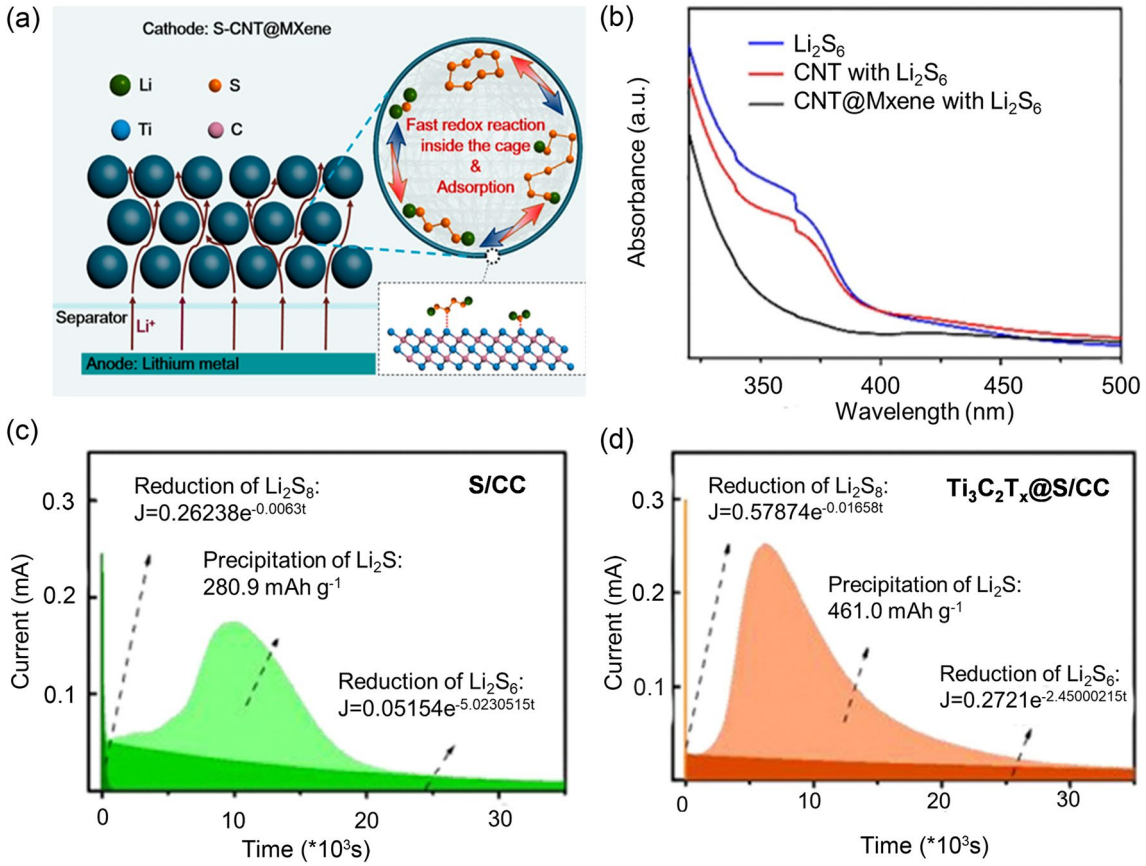

Fig. 12 **a** Schematic illustration of the synthesis of 3D S-CNT@MXene cage spheres. **b** UV/vis spectra of the Li_2S_6, CNT with Li_2S_6 and CNT@MXene with Li_2S_6. **a**, **b** Reproduced with permission from Ref. [162], Copyright 2021, Elsevier. Reduction of Li_2S_8/Li_2S_6 and precipitation of Li_2S during potentiostatic discharge of the Li_2S_8/tetraglyme catholyte on **c** CC and **d** $Ti_3C_2T_x$@CC at 2.05 V. **c**, **d** Reproduced with permission from Ref. [163], Copyright 2021, Elsevier

and LiPSs (Fig. 12b). Yin et al. synthesized S-impregnated carbon cloth cathode covered with $Ti_3C_2T_x$ flakes ($Ti_3C_2T_x$@S/CC) [163]. The $Ti_3C_2T_x$ layer not only physically confines the LiPSs but also chemically interacts with them due to its hydroxyl group to form surface thiosulfate species, which traps LiPSs and converts them directly into Li_2S through disproportionation. Also, the exposed acid Ti sites on the $Ti_3C_2T_x$ can strongly adsorb LiPSs through the formation of Ti-S bonds, further promoting the direct nucleation of Li_2S. Consequently, the Li_2S precipitation capacity of $Ti_3C_2T_x$@CC (461.0 mAh g^{-1}) (Fig. 12c) is higher than that of CC (280.9 mAh g^{-1}) (Fig. 12d).

Despite the strong anchoring ability of MXene to LSBs at the cathode–electrolyte interface, it is susceptible to oxidation in water and air due to the exposed metal atoms, leading to changes in properties [164, 165]. Therefore, improving its stability is an urgent problem that needs to be solved.

In the conventional solid–liquid–solid three-phase conversion mechanism, the troublesome shuttle effect begins at the liquid-phase transition stage. Therefore, the common ground these tactics have is they all aim to relieve the influence of the dissolution of the soluble LiPSs at the cathode–electrolyte interface and have made remarkable progress in the laboratory condition. However, they could only limit the shuttling of LiPSs but could not eliminate the liquid-phase transition.

3.2.2 Transformation from Solid–Liquid–Solid Pathway to Solid–Solid Pathway

In contrast to the solid–liquid–solid reaction mechanism, which involves anchoring the LiPSs through physical or chemical operations to suppress the shuttle effect as much as

https://doi.org/10.1007/s40820-024-01573-4

possible, the transition from a solid–liquid–solid pathway to a solid–solid pathway is anticipated to eliminate the shuttle effect. The process of achieving this transition is that a small amount of LiPSs is produced during the initial reduction stage, and subsequently the electrolyte reacts swiftly with LiPSs or undergoes in situ polymerization to form a dense CEI layer. As a result, a complete physical isolation of S from the electrolyte is achieved, and the redox pathway of S is transformed from the solvation–deposition mechanism to a solid-phase mechanism. In the mechanism, it becomes evident that the liquid–solid–solid reaction predominantly generates a dense CEI layer through electrolyte modification.

Carbonates, such as EC [114], diethyl carbonate (DEC) [166], and VC [167], can interact with LiPSs by nucleophilic reaction, resulting in the formation of polycarbonate organic precipitates with strong capabilities to impede the dissolution of LiPSs. The CEI layer composed of polycarbonate organic substances deposited on the cathode surface can achieve good physical isolation between the cathode and electrolyte, allowing only Li^+ to pass through and access the interior of cathode. Subsequently, the S conversion mechanism transitions into a solid–solid route. Reflected in the cyclic voltammetry (CV) curves, the redox peaks corresponding to the solid–liquid reaction gradually disappear and only solid-phase reaction maintains by following the formation of CEI layer, indicating complete inhibition of the LiPSs generation, as depicted in Fig. 13a [114]. Due to the nucleophilic reaction between carbonate compounds and LiPSs, this unique solid-phase transformation mechanism demonstrates high reversible cycle performance. A LSB utilizing S/C_{FS} as a cathode and VC acts as a co-solvent and exhibits outstanding charge/discharge characteristics with an original capacity of 1557 mAh g^{-1} and a peak cycling efficiency of 99.9% over 500 cycles [167].

Localized high-concentration carbonate electrolyte (LHCE) represents another way to harness carbonate solvents which are acquired by adding an inert diluent to the high-concentration electrolytes (HCEs). The reduced viscosity and improved ionic conductivity resulting from inert diluents can maintain the advantages of HCEs in forming a dense CEI layer [168]. For example, He et al. added the 1,1,2,2-tetrafluoroethyl-2,2,3,3-tetrafluoropropyl ether (TTE) to a DEC/FEC + LiTFSI system and created a LHCE (Fig. 13b) [166]. The addition of TTE does not coordinate with Li^+ but the electrolyte dilution promotes Li^+ migration. During the early stage of discharge, the nucleophilic reaction between carbonate and LiPSs gives rise to a CEI layer that exclusively allows only Li^+ to pass through, and S and Li^+ are directly converted to Li_2S/Li_2S_2 without further generation of LiPSs (Fig. 13c). As shown in Fig. 13d, the analysis of the S-k edge spectra and XPS spectra reveals that KB/S cathode undergoes a solid-phase conversion with the formation of a CEI layer comprising insoluble inorganics ($LiCO_3$ and LiF) and thiocarbonates on the electrode surface. However, it should be noted that the excessive diluent may decrease the proportion of carbonate, altering the solvent structure and impacting ionic transport, thus affecting the availability of active material.

In conventional dilute ether electrolytes, the S transition entails a solid–liquid–solid pathway involving the generation and dissolution of LiPSs, resulting in obvious shuttle effect. However, ether electrolytes with low solubility toward LiPSs are beneficial for maintaining stable interfacial phases. Chen et al. utilized a non-toxic and non-flammable dipropylene glycol dimethyl ether (DPGDME) as the solvent [169]. DPGDME can be in situ electrochemically polymerized during cycling and deepened with the cycling continuance, resulting in abundant polyethers on the cathode surface that builds an elastic CEI layer with low impedance (Fig. 13e) for fast Li^+ diffusion. The low LiPSs solubility of the polymer effectively maintains the solid–solid conversion, ensuring high capacity (1645.3 mAh g^{-1} based on S), excellent cycling stability (99.5% retention over 400 cycles), and ultrahigh average coulombic efficiency (CE) over 99.9995%. Ma et al. proposed low-cost and low-density weakly solvated electrolytes based on butyl methyl ether (BME) with low solvation power [170]. Compared with common ether solvents, the single ether O-bond of BME results in a lower electron donation, which reduces the coordination capacity of BME and the solubility of LiPSs in BME solvents (Fig. 13f). The lower coordination ability causes the solvation shell of the electrolyte to be dominated by FSI^-, which together with LiPSs forms stable CEI layer, effectively preventing LiPSs from dissolving and shuttling to the electrolyte, thereby realizing the solid–solid conversion (Fig. 13g).

Although a solid–solid pathway can be modulated with an organic-dominated CEI layer and exhibits excellent sealing to the cathode, the rate performance of the LSBs is relatively poor compared with dissolved-deposition mechanism. To improve the overall performance in the future, therefore, it may be considered to construct an organic–inorganic hybridized CEI layer, of which the crucial part is accurately

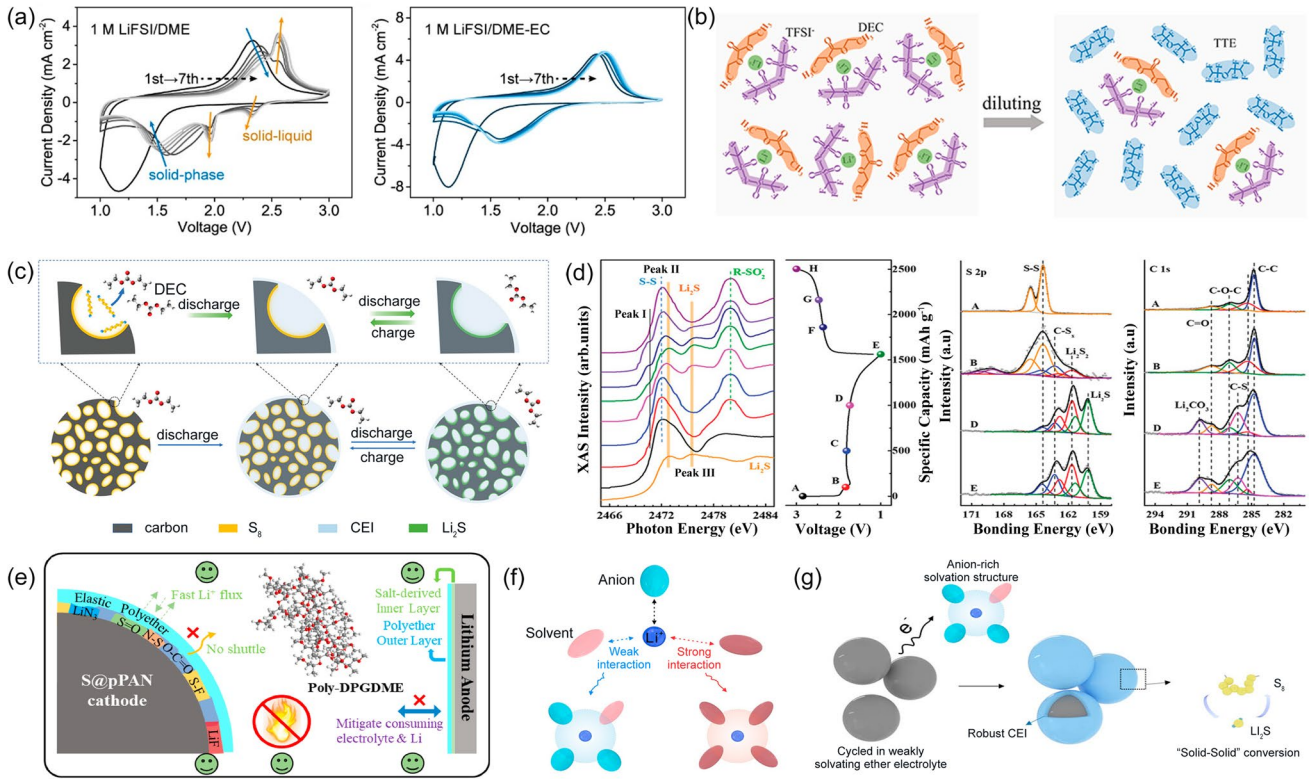

Fig. 13 **a** CV curves of the Li-SPAN half cells in 1 M LiFSI/DME and 1 M LiFSI/DME-EC electrolytes, respectively. Reproduced with permission from Ref. [114], Copyright 2021, American Chemical Society. **b** Solvate structure illustrations of the HCE (left) of LiTFSI + DEC and the LHCE (right) of LiTFSI + DEC + TTE, in which the LiTFSI, DEC, and TTE are used as examples for salt, solvent, and diluent, respectively. **c** Schematic illustration of the in situ formation of the CEI layer on the KB/S surfaces in the localized high-concentration carbonate-based electrolyte. **d** S K-edge spectra of KB/S electrodes in the carbonate LHCE at given discharge/charge steps and the corresponding GCD curve of the cell; XPS spectra of the electrode at given discharge states: S 2*p*, C 1*s*. **b**-**d** Reproduced with permission from Ref. [166], Copyright 2021, John Wiley and Sons. **e** The superiorities of the proposed DPGDME electrolyte toward both electrodes. Reproduced with permission from Ref. [169], Copyright 2022, Elsevier. **f** Illustration of Li^+-solvent interactions. **g** Conversion mechanism of SPAN in weakly solvating ether electrolyte. **f**, **g** Reproduced with permission from Ref. [170], Copyright 2023, John Wiley and Sons

controlling the ratio of organic and inorganic components. The success of new ether-based electrolyte demonstrates that regulating the solvation structure through proper selection of salts and solvents is an acceptable means to establish a hard-closed CEI layer to realize the solid–solid conversion.

3.2.3 Avoiding LiPSs Generation Through All-Solid–Solid Reaction

Compared with the above-mentioned reaction transition from solid–liquid–solid to solid–solid, the all-solid–solid conversion mechanism exclusively refers to the solid-phase conversion of S without the formation of any soluble LiPSs and can completely eliminate the shuttle effect. There are two main routes to achieve this. One is to directly sever the contact between S and electrolyte by establishing spatial restrictions at the cathode–electrolyte interface before cycling, while the other entails forming S-containing composites as the active substance through covalent bonding.

Employing a suitable layer represents an effective means of creating a physical separation at the cathode-interface. Owing to the precise control over the thickness and chemical composition on a molecular scale, molecular layer deposition (MLD) enables the creation of an effective separation layer on the cathode surface. For instance, Li et al. deposited a Li^+ accessible alucone film on the surface of C/S cathode via MLD [171]. The alucone film effectively achieved physical isolation between the cathode and carbonate electrolyte, forming a stable interface and preventing side reactions (Fig. 14a). During cycling, the cyclo-S_8 in

 https://doi.org/10.1007/s40820-024-01573-4

the conductive carbon matrix was directly converted to Li_2S through a solid-phase redox reaction rather than the complex solid–liquid–solid conversion (Fig. 14b). Another route involves electrolyte modulation for in situ CEI formation. Guo et al. developed an electrolyte additive of 1,3,5-benzenetrithiol (BTT), which combined with S alone or in pairs to react with Li^+, producing Li_2S_x on the cathode surface and lithium benzene trithiol (Li_3-BTT) on the anode surface, respectively (Fig. 14c) [172]. This interfacial reaction differs from the usual in situ reaction independent of LiPSs generated in the early cycles, instead of the in situ direct oligomerization of BTT and S forming a chemically and mechanically stable solid CEI layer. Based on this unique redox pathway fundamentally inhibiting the LiPSs production, the first discharge capacity is 1036 mAh g^{-1} at 1 C and maintains 907 mAh g^{-1} even after 300 cycles with 87.6% capacity retention.

Yi et al. thermally synthesized a graphdiyne-like porous organic framework (GPOF), of which highly active acetylene bonds reacted with S within the micropores at high temperature, forming a sulfide compound of SGPOF with C–S–S–C chains [173]. The short chains chemically react with the unsaturated carbon atoms of the GPOF through covalent bonding (Fig. 14d), resulting in only the solid-phase transformations among the low-molecular-weight sulfides and thereby eliminating the LiPSs generation at the cathode–electrolyte interface. When S is covalently immobilized on the triallyl isocyanurate to synthesize S-triallyl isocyanurate organosulfur polymer composites (STIs) that are used as actives, the triallyl monomer and S will form a cyclic structure embedded with short polysulfur chain, avoiding detrimental transitions of the long-chain LiPSs in the discharge/charging process (Fig. 14e) [174]. Under high S loading (4.5 mg cm^{-2}) and low S electrolyte (8 uL mg^{-1}) conditions, the pouch cell showed almost no capacity degradation over 125 cycles. Zhang et al. prepared polymers with a high S content containing disulfide chains (DSP) and trisulfide chains (TSP) as novel active materials for LSBs [175]. As shown in Fig. 14f, DFT calculations showed that the DSP and the TSP have different lithiation products and reaction pathways from the monolithic S, avoiding the generation of LiPSs during the conversion process and providing a stable cathode–electrolyte interface. The solid–solid conversion mechanism can be realized through spatial confinement but requires the preparation process as a pressing subject. In contrast, S-containing composites are easier to commercialize and it is feasible to explore composites with higher S content.

4 Summaries and Prospects

LSBs with high specific capacity and low cost are viewed as one of the most promising candidates for the post-LIBs era. However, there are still a lot of cathode–electrolyte interface issues, such as shuttle effect and the structural changes, momentarily left in suspense impeding their practical application. To tackle the obstacles, manipulating the interface is gradually paid more and more attention. In this review, a thorough and systematic understanding of cathode–electrolyte interface issues and the corresponding state-of-the-art strategies are presented (Fig. 15) and well discussed. The strategies are classified according to the perspectives of structural enhancement and reaction mechanisms.

The CEI layer and deposition pattern of Li_2S are directly connected to the stability of the cathode–electrolyte interface. Their optimal method also has a resemblance to adding electrolyte additives. It is worth mentioning that adding proper electrolyte additives could promote the formation of a CEI layer. The mechanism of how the CEI layer responds to certain additives should be further expanded in the future to direct the rational design of electrolyte additives. Either increasing the solubility or regulating the deposition pattern of Li_2S proves favorable and effective. The high DN solvents can serve as the electrolyte to not only increase the solubility of Li_2S but also stabilize the short-chain LiPSs to provide a novel deposition pathway. In particular, metal-based materials can promote the 3D deposition of Li_2S while avoiding corrosion of the lithium metal anode that occurs in high DN electrolyte systems. However, the 3D deposition of Li_2S on metal substrates comes at the expense of catalytic sites, so it needs further exploration on how to maintain the catalytic activity of the interface.

The dissolution of the LiPSs at the cathode–electrolyte interface that triggers the subsequent shuttle effect can lead to damage in both electrodes and capacity decline. In recent years, studies have shown that the traditional "solid–liquid–solid" mechanism can be modulated to inhibit the shuttle effect. The common strategy is adopting various materials to modify the cathode interface to restrain the LiPSs from shuttling. The option varies from functional carbon, polymers with rich polar functional groups, and polar metal

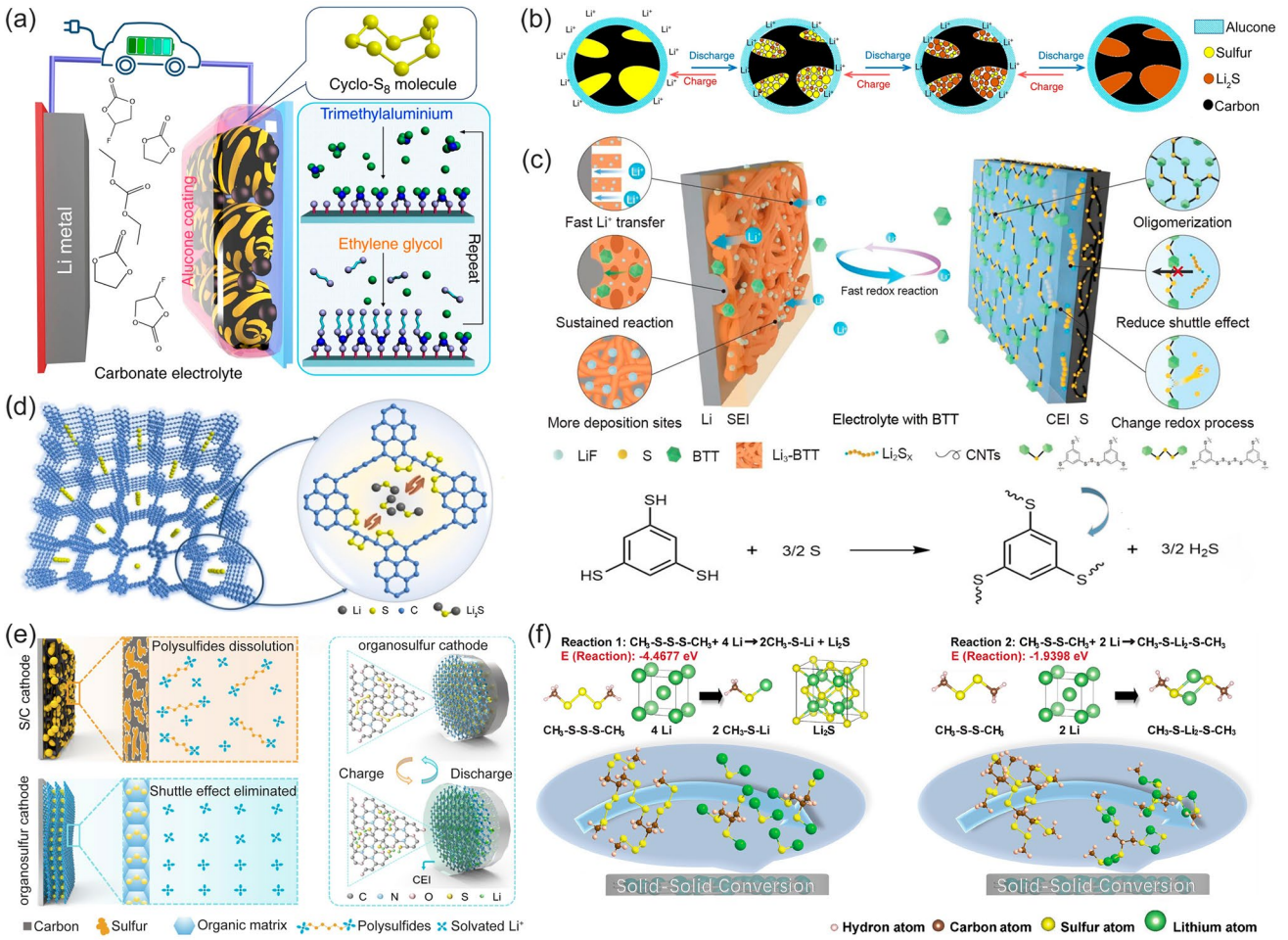

Fig. 14 **a** Schematic diagram of alucone coating on carbon/S (ring-S_8) cathode and **b** proposed reaction mechanism in the carbonate electrolyte. **a**, **b** Reproduced with permission from Ref. [171], Copyright 2018, Springer Nature. **c** D-SEIs are formed on the interfaces of the anode and cathode. Reproduced with permission from Ref. [172], Copyright 2021, Springer Nature. **d** Schematic diagram of the SGPOF with a short S-chain. Reproduced with permission from Ref. [173], Copyright 2021, American Chemical Society. **e** Schematic structures of S/C cathode following solid–liquid–solid reaction with LiPSs dissolution (above) and the organosulfur cathode (below) following solid–solid reaction with eliminated shuttle effect, as well as the structural reorganization of organosulfur cathode during the reaction process. Reproduced with permission from Ref. [174], Copyright 2023, Elsevier. **f** Calculation of energy changes of possible lithiation reactions, bond length, and reaction formula for CH_3–S–S–S–CH_3 (Reaction 1) and CH_3–S–S–CH_3 (Reaction 2), and their proposed electrochemical conversions. Reproduced with permission from Ref. [175], Copyright 2022, Elsevier

compounds to MXenes. However, they could only mitigate the shuttle effect not eliminate it. The common ground these methods share is to avoid the dissolution of the LiPSs into the electrolyte, and some novel methods to regulate the reaction mechanism are under the same idea to avoid the liquid-phase transition at the cathode–electrolyte interface which can restrain the shuttle effect from the root. The transformation from the solid–liquid–solid pathway to the solid–solid pathway is achieved through the electrolyte modification, and the solid–solid reaction pathway can generally be modulated by either spatial restrictions between the cathode and electrolyte or the covalent bonding of the S-containing composites.

We believe that a full understanding of the cathode–electrolyte interface behavior is the key to improving the overall performance of the LSBs. Recently, it has been paid more and more attention. The insight into the reaction mechanism given by Sun et al. for the first time shed light on the collective mechanism [176]. More insightful work is required to look into the reaction behavior at the cathode–electrolyte interface.

https://doi.org/10.1007/s40820-024-01573-4

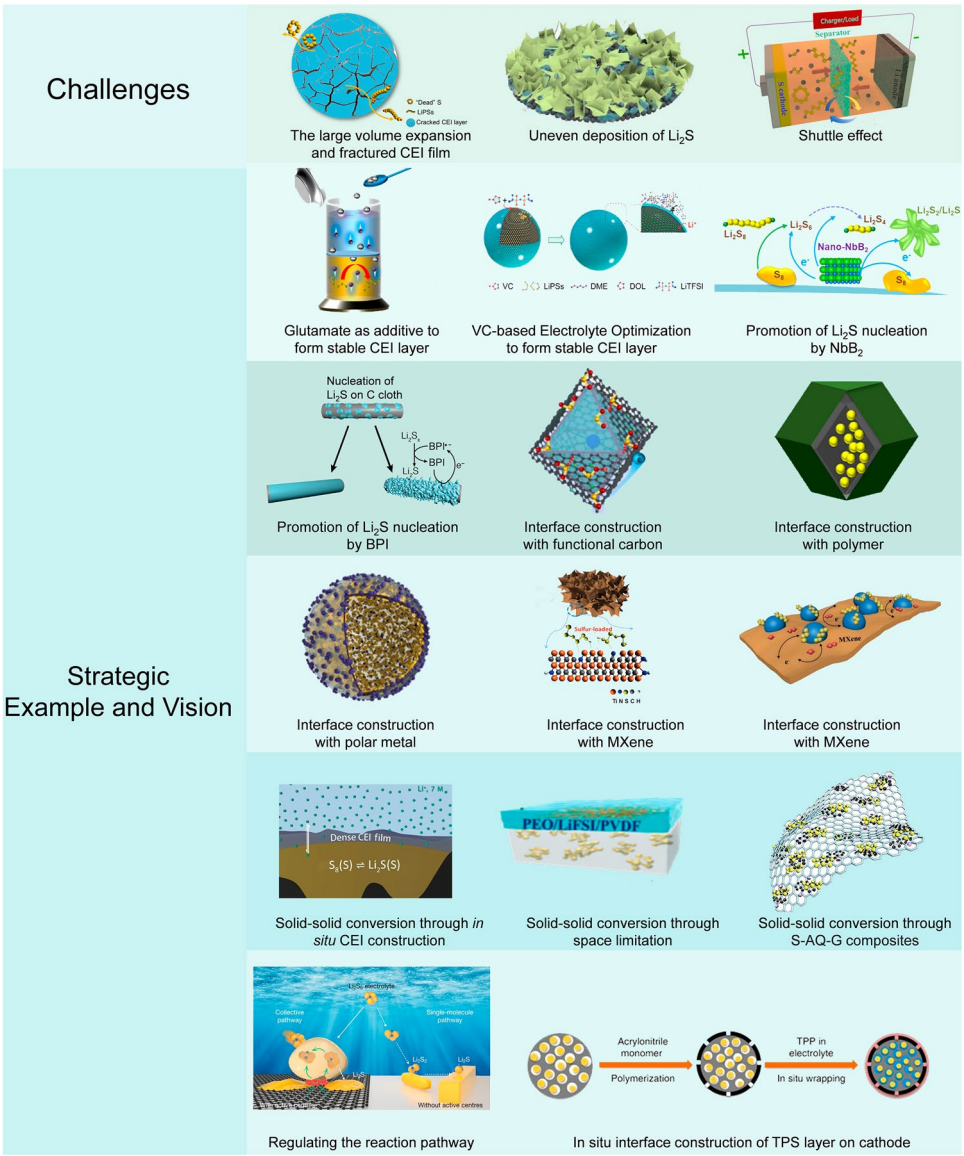

Fig. 15 The challenges, strategic examples, and novel visions of the electrode–electrolyte interface of LSBs. Reproduced with permission from Ref. [177], Copyright 2023, Elsevier; Ref. [178], Copyright 2021, Elsevier; Ref. [179], Copyright 2019, American Chemical Society; Ref. [115], Copyright 2023, John Wiley and Sons; Ref. [180], Copyright 2022, American Chemical Society; Ref. [181], Copyright 2016, American Chemical Society; Ref. [128], Copyright 2021, Springer Nature; Ref. [182], Copyright 2023, MDPI; Ref. [183], Copyright 2020, Springer Nature; Ref. [184], Copyright 2018, Springer Nature; Ref. [160], Copyright 2019, Springer Nature; Ref. [185], Copyright 2023, Springer Nature; Ref. [186], Copyright 2023, Springer Nature; Ref. [187], Copyright 2018, Springer Nature; Ref. [176], Copyright 2019, Springer Nature; and Ref. [188], Copyright 2019, Springer Nature

Although the aforementioned strategies have proved useful for obtaining a stable cathode–electrolyte interface of LSBs, a versatile method with both economic feasibility and environmental friendliness is still a long haul. The novel vision of the cathode–electrolyte interface still needs further exploration. The good news is that the fundamental issues at the interface have drawn more and more attention. It is believed that, with the ongoing development and strides of electrochemistry and material science, the cathode–electrolyte interface issues will be eventually optimized and the stable operation of LSBs can be prolonged and tap their full potential for wide commercialization.

Acknowledgements This work was supported by the National Natural Science Foundation of China (Grant Nos. 52102302, 22409161 and 52472249), the Young Talent Support Plan of Xi'an Jiaotong University (Grant No. DQ6J011), the Natural Science Foundation of Shaanxi Province (2023-JC-QN-0115) and the China Postdoctoral Science Foundation (2022M712499), and Beilin District Science and Technology Plan (GX2328). Prof. P.-F. Wang also thanks the support from Young Elite Scientists Sponsorship Program by Chinese Association for Science and Technology, the "High-Level Talent Introduction Plan" of Shaanxi Province and Siyuan Scholar of Xi'an Jiaotong University.

Author Contributions ML and LH contributed to conceptualization, investigation, and original draft writing. ZG was involved in investigation and visualization. T-LC, X-YZ, and SS contributed to visualization. RS was involved in review. PJ and P-FW contributed to conceptualization, reviewing and editing writing, funding acquisition, supervision, and resources.

Declarations

Conflict of interest The authors declare no interest conflict. They have no known competing financial interests or personal relationships that could have appeared to influence the work reported in this paper.

References

1. B.J. van Ruijven, E. DeCian, I. SueWing, Amplification of future energy demand growth due to climate change. Nat. Commun. **10**, 2762 (2019). https://doi.org/10.1038/s41467-019-10399-3
2. W. Gao, Z. Wang, C. Peng, S. Kang, L. Cui, Accelerating the redox kinetics by catalytic activation of "dead sulfur" in lithium–sulfur batteries. J. Mater. Chem. A **9**, 13442–13458 (2021). https://doi.org/10.1039/d1ta00772f
3. Z. Zhuang, J. Huang, Y. Li, L. Zhou, L. Mai, The holy grail in platinum-free electrocatalytic hydrogen evolution: molybdenum-based catalysts and recent advances. ChemElectroChem **6**, 3570–3589 (2019). https://doi.org/10.1002/celc.201900143
4. S.-J. Kim, K. Kim, J. Park, Y.-E. Sung, Role and potential of metal sulfide catalysts in lithium-sulfur battery applications. ChemCatChem **11**, 2373–2387 (2019). https://doi.org/10.1002/cctc.201900184
5. Z. Zhuang, Q. Kang, D. Wang, Y. Li, Single-atom catalysis enables long-life, high-energy lithium-sulfur batteries. Nano Res. **13**, 1856–1866 (2020). https://doi.org/10.1007/s12274-020-2827-4
6. G. Zhou, H. Chen, Y. Cui, Formulating energy density for designing practical lithium–sulfur batteries. Nat. Energy **7**, 312–319 (2022). https://doi.org/10.1038/s41560-022-01001-0
7. D. Wang, N. Liu, F. Chen, Y. Wang, J. Mao, Progress and prospects of energy storage technology research: based on multidimensional comparison. J. Energy Storage **75**, 109710 (2024). https://doi.org/10.1016/j.est.2023.109710
8. N. Kittner, F. Lill, D.M. Kammen, Energy storage deployment and innovation for the clean energy transition. Nat. Energy **2**, 17125 (2017). https://doi.org/10.1038/nenergy.2017.125
9. D. Liu, Z. Shadike, R. Lin, K. Qian, H. Li et al., Review of recent development of in situ/operando characterization techniques for lithium battery research. Adv. Mater. **31**, e1806620 (2019). https://doi.org/10.1002/adma.201806620
10. B. Scrosati, J. Garche, Lithium batteries: status, prospects and future. J. Power. Sources **195**, 2419–2430 (2010). https://doi.org/10.1016/j.jpowsour.2009.11.048
11. M.V. Reddy, A. Mauger, C.M. Julien, A. Paolella, K. Zaghib, Brief history of early lithium-battery development. Materials **13**, 1884 (2020). https://doi.org/10.3390/ma13081884
12. L. Trahey, F.R. Brushett, N.P. Balsara, G. Ceder, L. Cheng et al., Energy storage emerging: a perspective from the joint center for energy storage research. Proc. Natl. Acad. Sci. U.S.A. **117**, 12550–12557 (2020). https://doi.org/10.1073/pnas.1821672117
13. J. Xie, Y.-C. Lu, A retrospective on lithium-ion batteries. Nat. Commun. **11**, 2499 (2020). https://doi.org/10.1038/s41467-020-16259-9
14. Y. Lu, J. Chen, Prospects of organic electrode materials for practical lithium batteries. Nat. Rev. Chem. **4**, 127–142 (2020). https://doi.org/10.1038/s41570-020-0160-9
15. J. Liu, J. Wang, Y. Ni, K. Zhang, F. Cheng et al., Recent breakthroughs and perspectives of high-energy layered oxide cathode materials for lithium ion batteries. Mater. Today **43**, 132–165 (2021). https://doi.org/10.1016/j.mattod.2020.10.028
16. J.W. Choi, D. Aurbach, Promise and reality of post-lithium-ion batteries with high energy densities. Nat. Rev. Mater. **1**, 16013 (2016). https://doi.org/10.1038/natrevmats.2016.13
17. L. Chen, G. Cao, Y. Li, G. Zu, R. Duan et al., A review on engineering transition metal compound catalysts to accelerate the redox kinetics of sulfur cathodes for lithium-sulfur batteries. Nano-Micro Lett. **16**, 97 (2024). https://doi.org/10.1007/s40820-023-01299-9

18. C. Sun, X. Zhang, C. Li, K. Wang, X. Sun et al., Recent advances in prelithiation materials and approaches for lithium-ion batteries and capacitors. Energy Storage Mater. **32**, 497–516 (2020). https://doi.org/10.1016/j.ensm.2020.07.009
19. X. Yu, W. Li, V. Gupta, H. Gao, D. Tran et al., Current challenges in efficient lithium-ion batteries' recycling: a perspective. Glob. Chall. **6**, 2200099 (2022). https://doi.org/10.1002/gch2.202200099
20. J. Li, Z. Niu, C. Guo, M. Li, W. Bao, Catalyzing the polysulfide conversion for promoting lithium sulfur battery performances: a review. J. Energy Chem. **54**, 434–451 (2021). https://doi.org/10.1016/j.jechem.2020.06.009
21. W.-M. Zhao, J.-D. Shen, X.-J. Xu, W.-X. He, L. Liu et al., Functional catalysts for polysulfide conversion in Li–S batteries: from micro/nanoscale to single atom. Rare Met. **41**, 1080–1100 (2022). https://doi.org/10.1007/s12598-021-01865-3
22. Z.P. Cano, D. Banham, S. Ye, A. Hintennach, J. Lu et al., Batteries and fuel cells for emerging electric vehicle markets. Nat. Energy **3**, 279–289 (2018). https://doi.org/10.1038/s41560-018-0108-1
23. C. Yang, Running battery electric vehicles with extended range: coupling cost and energy analysis. Appl. Energy **306**, 118116 (2022). https://doi.org/10.1016/j.apenergy.2021.118116
24. M.C. Argyrou, P. Christodoulides, S.A. Kalogirou, Energy storage for electricity generation and related processes: technologies appraisal and grid scale applications. Renew. Sustain. Energy Rev. **94**, 804–821 (2018). https://doi.org/10.1016/j.rser.2018.06.044
25. H. Pan, Z. Cheng, Z. Zhou, S. Xie, W. Zhang et al., Boosting lean electrolyte lithium-sulfur battery performance with transition metals: a comprehensive review. Nano-Micro Lett. **15**, 165 (2023). https://doi.org/10.1007/s40820-023-01137-y
26. P. Wang, B. Xi, M. Huang, W. Chen, J. Feng et al., Emerging catalysts to promote kinetics of lithium–sulfur batteries. Adv. Energy Mater. **11**, 2002893 (2021). https://doi.org/10.1002/aenm.202002893
27. R. Deng, H. Yu, J. Liu, F. Chu, J. Lei et al., Adsorption-catalytic effects of metallurgical ferrous slag on polysulfides in Li–S batteries. J. Mater. Chem. A **11**, 15769–15777 (2023). https://doi.org/10.1039/d3ta02327c
28. Y. Chen, T. Wang, H. Tian, D. Su, Q. Zhang et al., Advances in lithium–sulfur batteries: from academic research to commercial viability. Adv. Mater. **33**, 2003666 (2021). https://doi.org/10.1002/adma.202003666
29. C. Deng, X. Li, R. Chen, K. Ye, J. Lipton et al., Recent advances in rocking chair batteries and beyond. Energy Storage Mater. **60**, 102820 (2023). https://doi.org/10.1016/j.ensm.2023.102820
30. F. Su, J. Qin, P. Das, F. Zhou, Z.-S. Wu, A high-performance rocking-chair lithium-ion battery-supercapacitor hybrid device boosted by doubly matched capacity and kinetics of the faradaic electrodes. Energy Environ. Sci. **14**, 2269–2277 (2021). https://doi.org/10.1039/D1EE00317H
31. P. Jing, M. Liu, H.-P. Ho, Y. Ma, W. Hua et al., Tailoring the Wadsley-Roth crystallographic shear structures for high-power lithium-ion batteries. Energy Environ. Sci. **17**, 6571–6581 (2024). https://doi.org/10.1039/d4ee02293a
32. M. Liu, B. Wu, D. Si, H. Dong, K. Chen et al., Electronic states tailoring and pinning effect boost high-power sodium-ion storage of oriented hollow P2-type cathode materials. ACS Appl. Mater. Interfaces **15**, 53623–53631 (2023). https://doi.org/10.1021/acsami.3c14951
33. M. Liu, Z. Cheng, X. Zhu, H. Dong, T. Yan et al., Biphase-to-monophase structure evolution of $Na_{0.766+x}Li_xNi_{0.33-x}Mn_{0.5}Fe_{0.1}Ti_{0.07}O_2$ toward ultradurable Na-ion batteries. Carbon Energy **6**, e565 (2024). https://doi.org/10.1002/cey2.565
34. S. Lang, S.-H. Yu, X. Feng, M.R. Krumov, H.D. Abruña, Understanding the lithium-sulfur battery redox reactions via operando confocal Raman microscopy. Nat. Commun. **13**, 4811 (2022). https://doi.org/10.1038/s41467-022-32139-w
35. R. Deng, M. Wang, H. Yu, S. Luo, J. Li et al., Recent advances and applications toward emerging lithium–sulfur batteries: working principles and opportunities. Energy Environ. Mater. **5**, 777–799 (2022). https://doi.org/10.1002/eem2.12257
36. R. Chu, T.T. Nguyen, Y. Bai, N.H. Kim, J.H. Lee, Uniformly controlled treble boundary using enriched adsorption sites and accelerated catalyst cathode for robust lithium–sulfur batteries. Adv. Energy Mater. **12**, 2102805 (2022). https://doi.org/10.1002/aenm.202102805
37. Q. Shao, S. Zhu, J. Chen, A review on lithium-sulfur batteries: challenge, development, and perspective. Nano Res. **16**, 8097–8138 (2023). https://doi.org/10.1007/s12274-022-5227-0
38. W. Sun, Z. Song, Z. Feng, Y. Huang, Z.J. Xu et al., Carbon-nitride-based materials for advanced lithium-sulfur batteries. Nano-Micro Lett. **14**, 222 (2022). https://doi.org/10.1007/s40820-022-00954-x
39. J. Sun, Y. Liu, L. Liu, S. He, Z. Du et al., Expediting sulfur reduction/evolution reactions with integrated electrocatalytic network: a comprehensive kinetic map. Nano Lett. **22**, 3728–3736 (2022). https://doi.org/10.1021/acs.nanolett.2c00642
40. C. Tong, H. Chen, S. Jiang, L. Li, M. Shao et al., Suppress loss of polysulfides in lithium-sulfur battery by regulating the rate-determining step via 1T MoS_2-MnO_2 covering layer. ACS Appl. Mater. Interfaces **15**, 1175–1183 (2023). https://doi.org/10.1021/acsami.2c18594
41. M. Zhen, K. Li, M. Liu, Manipulating Li_2 S redox kinetics and lithium dendrites by core-shell catalysts under high sulfur loading and lean-electrolyte conditions. Adv. Sci. **10**, e2207442 (2023). https://doi.org/10.1002/advs.202207442
42. S. Waluś, G. Offer, I. Hunt, Y. Patel, T. Stockley et al., Volumetric expansion of lithium-sulfur cell during operation–fundamental insight into applicable characteristics. Energy Storage Mater. **10**, 233–245 (2018). https://doi.org/10.1016/j.ensm.2017.05.017
43. R. Chen, Y. Zhou, X. Li, Nanocarbon-enabled mitigation of sulfur expansion in lithium–sulfur batteries. Energy Storage

Mater. **68**, 103353 (2024). https://doi.org/10.1016/j.ensm.2024.103353

44. Y. He, Z. Chang, S. Wu, Y. Qiao, S. Bai et al., Simultaneously inhibiting lithium dendrites growth and polysulfides shuttle by a flexible MOF-based membrane in Li–S batteries. Adv. Energy Mater. **8**, 1802130 (2018). https://doi.org/10.1002/aenm.201802130
45. C.-X. Bi, L.-P. Hou, Z. Li, M. Zhao, X.-Q. Zhang et al., Protecting lithium metal anodes in lithium–sulfur batteries: a review. Energy Mater. Adv. **4**, 0010 (2023). https://doi.org/10.34133/energymatadv.0010
46. Q. Zhao, S. Stalin, L.A. Archer, Stabilizing metal battery anodes through the design of solid electrolyte interphases. Joule **5**, 1119–1142 (2021). https://doi.org/10.1016/j.joule.2021.03.024
47. M. Chen, M. Shao, J. Jin, L. Cui, H. Tu et al., Configurational and structural design of separators toward shuttling-free and dendrite-free lithium-sulfur batteries: a review. Energy Storage Mater. **47**, 629–648 (2022). https://doi.org/10.1016/j.ensm.2022.02.051
48. W. Li, H. Yao, K. Yan, G. Zheng, Z. Liang et al., The synergetic effect of lithium polysulfide and lithium nitrate to prevent lithium dendrite growth. Nat. Commun. **6**, 7436 (2015). https://doi.org/10.1038/ncomms8436
49. L. Qie, C. Zu, A. Manthiram, A high energy lithium-sulfur battery with ultrahigh-loading lithium polysulfide cathode and its failure mechanism. Adv. Energy Mater. **6**, 1502459 (2016). https://doi.org/10.1002/aenm.201502459
50. M. Liu, S. Jhulki, Z. Sun, A. Magasinski, C. Hendrix et al., Atom-economic synthesis of Magnéli phase Ti_4O_7 microspheres for improved sulfur cathodes for Li–S batteries. Nano Energy **79**, 105428 (2021). https://doi.org/10.1016/j.nanoen.2020.105428
51. R. Yan, M. Oschatz, F. Wu, Towards stable lithium-sulfur battery cathodes by combining physical and chemical confinement of polysulfides in core-shell structured nitrogen-doped carbons. Carbon **161**, 162–168 (2020). https://doi.org/10.1016/j.carbon.2020.01.046
52. F. Wu, H. Lv, S. Chen, S. Lorger, V. Srot et al., Natural vermiculite enables high-performance in lithium–sulfur batteries via electrical double layer effects. Adv. Funct. Mater. **29**, 1902820 (2019). https://doi.org/10.1002/adfm.201902820
53. Z. Song, W. Jiang, B. Li, Y. Qu, R. Mao et al., Advanced polymers in cathodes and electrolytes for lithium-sulfur batteries: progress and prospects. Small **20**, e2308550 (2024). https://doi.org/10.1002/smll.202308550
54. W. Liu, Y. Chu, J. Zhou, X. Chen, Y. Wang et al., A honeycomb-structured CoF_2-modified separator enabling high-performance lithium−sulfur batteries. Small Sci. **3**, 2300006 (2023). https://doi.org/10.1002/smsc.202300006
55. X. Yang, J. Liu, F. Chu, J. Lei, F. Wu, Separator modification by Mo_xC/N-doped graphene enabling polysulfide catalytic conversion for high-performance Li–S batteries. Mater. Today Energy **35**, 101318 (2023). https://doi.org/10.1016/j.mtener.2023.101318
56. M. Liu, S. Jhulki, A. Magasinski, P.-F. Wang, G. Yushin, Porous TiO_{2-x}/C nanofibers with axially aligned tunnel pores as effective sulfur hosts for stabilized lithium–sulfur batteries. ACS Appl. Mater. Interfaces **14**, 54725–54735 (2022). https://doi.org/10.1021/acsami.2c16578
57. W. Li, B. Yang, R. Pang, M. Zhang, Sandwiched aramid nanofiber/Al_2O_3-coated polyolefin separators for advanced lithium–sulfur batteries. Compos. Commun. **38**, 101489 (2023). https://doi.org/10.1016/j.coco.2022.101489
58. Y. Li, T. Gao, D. Ni, Y. Zhou, M. Yousaf et al., Two birds with one stone: interfacial engineering of multifunctional Janus separator for lithium-sulfur batteries. Adv. Mater. **34**, e2107638 (2022). https://doi.org/10.1002/adma.202107638
59. J. Yan, F. Liu, Z. Hu, J. Gao, W. Zhou et al., Realizing dendrite-free lithium deposition with a composite separator. Nano Lett. **20**, 3798–3807 (2020). https://doi.org/10.1021/acs.nanolett.0c00819
60. R. Gao, M. Zhang, Z. Han, X. Xiao, X. Wu et al., Unraveling the coupling effect between cathode and anode toward practical lithium-sulfur batteries. Adv. Mater. **36**, e2303610 (2024). https://doi.org/10.1002/adma.202303610
61. S. Yuan, Q. Lai, X. Duan, Q. Wang, Carbon-based materials as anode materials for lithium-ion batteries and lithium-ion capacitors: a review. J. Energy Storage **61**, 106716 (2023). https://doi.org/10.1016/j.est.2023.106716
62. J. Chang, J. Shang, Y. Sun, L.K. Ono, D. Wang et al., Flexible and stable high-energy lithium-sulfur full batteries with only 100% oversized lithium. Nat. Commun. **9**, 4480 (2018). https://doi.org/10.1038/s41467-018-06879-7
63. W. Wang, X. Yue, J. Meng, J. Wang, X. Wang et al., Lithium phosphorus oxynitride as an efficient protective layer on lithium metal anodes for advanced lithium-sulfur batteries. Energy Storage Mater. **18**, 414–422 (2019). https://doi.org/10.1016/j.ensm.2018.08.010
64. S. Li, H. Dai, Y. Li, C. Lai, J. Wang et al., Designing Li-protective layer via $SOCl_2$ additive for stabilizing lithium-sulfur battery. Energy Storage Mater. **18**, 222–228 (2019). https://doi.org/10.1016/j.ensm.2018.09.012
65. E. Coleman, D.G. Li, H.F. Lv, R.Y. Wang, D. Strmcnik et al., Energy and fuels from tailored nanomaterials and electrochemical interfaces. Nat. Mater. **16**, 57–69 (2017). https://doi.org/10.1038/nmat4738
66. Y. Liu, Y. Elias, J. Meng, D. Aurbach, R. Zou et al., Electrolyte solutions design for lithium-sulfur batteries. Joule **5**, 2323–2364 (2021). https://doi.org/10.1016/j.joule.2021.06.009
67. L.L. Su, N. Yao, Z. Li, C.X. Bi, Z.X. Chen et al., Improving rate performance of encapsulating lithium-polysulfide electrolytes for practical lithium-sulfur batteries. Angew. Chem. Int. Ed. **63**, e202318785 (2024). https://doi.org/10.1002/anie.202318785
68. J. Kim, F. Zhao, L.K.S. Bonagiri, Q. Ai, Y. Zhang, Electrical double layers modulate the growth of solid–electrolyte interphases. Chem. Mater. **36**, 9156–9166 (2024). https://doi.org/10.1021/acs.chemmater.4c01745

 https://doi.org/10.1007/s40820-024-01573-4

69. Z. Guo, X. Song, X. Wang, C. Wang, X. An et al., Inhibition of polysulfide shuttling in high-polarity electrolytes via liquid/quasi-solid interface in lithium-sulfur batteries. Sci. China Mater. **66**, 505–512 (2023). https://doi.org/10.1007/s40843-022-2154-8
70. C. Xiao, W. Song, J. Liang, J. Zhang, Z. Huang et al., P-block tin single atom catalyst for improved electrochemistry in a lithium–sulfur battery: a theoretical and experimental study. J. Mater. Chem. A **10**, 3667–3677 (2022). https://doi.org/10.1039/D1TA09422J
71. R. Liu, J. Duay, S.B. Lee, Heterogeneous nanostructured electrode materials for electrochemical energy storage. Chem. Commun. **47**, 1384–1404 (2011). https://doi.org/10.1039/C0CC03158E
72. H. Su, Z. Xie, J. Feng, Q. Wang, J. Zhou et al., Electrolyte additive strategy enhancing the electrochemical performance of a soft-packed $LiCoO_2$// graphite full cell. Dalton Trans. **51**, 8723–8732 (2022). https://doi.org/10.1039/d2dt01088g
73. T. Wulandari, D. Fawcett, S.B. Majumder, G.E.J. Poinern, Lithium-based batteries, history, current status, challenges, and future perspectives. Battery Energy **2**, 20230030 (2023). https://doi.org/10.1002/bte2.20230030
74. M. Chen, S. Zhao, S. Jiang, C. Huang, X. Wang et al., Suppressing the polysulfide shuttle effect by heteroatom-doping for high-performance lithium–sulfur batteries. ACS Sustain. Chem. Eng. **6**, 7545–7557 (2018). https://doi.org/10.1021/acssuschemeng.8b00273
75. J.-H. Tian, T. Jiang, M. Wang, Z. Hu, X. Zhu et al., In situ/operando spectroscopic characterizations guide the compositional and structural design of lithium–sulfur batteries. Small Methods **4**, 1900467 (2020). https://doi.org/10.1002/smtd.201900467
76. Y. Huang, L. Lin, C. Zhang, L. Liu, Y. Li et al., Recent advances and strategies toward polysulfides shuttle inhibition for high-performance Li–S batteries. Adv. Sci. **9**, 2106004 (2022). https://doi.org/10.1002/advs.202106004
77. L. Wang, Y. Lin, S. DeCarlo, Y. Wang, K. Leung et al., Compositions and formation mechanisms of solid–electrolyte interphase on microporous carbon/sulfur cathodes. Chem. Mater. **32**, 3765–3775 (2020). https://doi.org/10.1021/acs.chemmater.9b05027
78. M. Helen, M. Fichtner, M.A. Reddy, Toward improving the areal energy density of lithium–sulfur batteries with ultramicroporous carbon–sulfur composite electrodes. Energy Technol. **7**, 1900183 (2019). https://doi.org/10.1002/ente.201900183
79. J. Zhang, S. Ma, J. Zhang, J. Zhang, X. Wang et al., Critical review on cathode electrolyte interphase towards stabilization for sodium-ion batteries. Nano Energy **128**, 109814 (2024). https://doi.org/10.1016/j.nanoen.2024.109814
80. Z. Zhang, J. Yang, W. Huang, H. Wang, W. Zhou et al., Cathode-electrolyte interphase in lithium batteries revealed by cryogenic electron microscopy. Matter **4**, 302–312 (2021). https://doi.org/10.1016/j.matt.2020.10.021
81. Y. Liao, H. Zhang, Y. Peng, Y. Hu, J. Liang et al., Electrolyte degradation during aging process of lithium-ion batteries: mechanisms, characterization, and quantitative analysis. Adv. Energy Mater. **14**, 2304295 (2024). https://doi.org/10.1002/aenm.202304295
82. Sungjemmenla, S.K. Vineeth, C.B. Soni, V. Kumar, Z.W. Seh, Understanding the cathode-electrolyte interphase in lithium-ion batteries. Energy Technol. **10**, 2200421 (2022). https://doi.org/10.1002/ente.202200421
83. H. Wang, X. Li, F. Li, X. Liu, S. Yang et al., Formation and modification of cathode electrolyte interphase: a mini review. Electrochem. Commun. **122**, 106870 (2021). https://doi.org/10.1016/j.elecom.2020.106870
84. F. Chu, M. Wang, J. Liu, Z. Guan, H. Yu et al., Low concentration electrolyte enabling cryogenic lithium–sulfur batteries. Adv. Funct. Mater. **32**, 2205393 (2022). https://doi.org/10.1002/adfm.202205393
85. R. Glaser, F. Wu, E. Register, M. Tolksdorf, B. Johnson et al., Tuning low concentration electrolytes for high rate performance in lithium-sulfur batteries. J. Electrochem. Soc. **167**, 100512 (2020). https://doi.org/10.1149/1945-7111/ab7183
86. X. Zhang, P. Gao, Z. Wu, M.H. Engelhard, X. Cao et al., Pinned electrode/electrolyte interphase and its formation origin for sulfurized polyacrylonitrile cathode in stable lithium batteries. ACS Appl. Mater. Interfaces **14**, 52046–52057 (2022). https://doi.org/10.1021/acsami.2c16890
87. T. Yim, M.-S. Park, J.-S. Yu, K.J. Kim, K.Y. Im et al., Effect of chemical reactivity of polysulfide toward carbonate-based electrolyte on the electrochemical performance of Li–S batteries. Electrochim. Acta **107**, 454–460 (2013). https://doi.org/10.1016/j.electacta.2013.06.039
88. H. Yang, J. Chen, J. Yang, J. Wang, Prospect of sulfurized pyrolyzed poly(acrylonitrile) (S@pPAN) cathode materials for rechargeable lithium batteries. Angew. Chem. Int. Ed. **59**, 7306–7318 (2020). https://doi.org/10.1002/anie.201913540
89. C. Kensy, D. Leistenschneider, S. Wang, H. Tanaka, S. Dörfler et al., The role of carbon electrodes pore size distribution on the formation of the cathode–electrolyte interphase in lithium–sulfur batteries. Batter. Supercaps **4**, 612–622 (2021). https://doi.org/10.1002/batt.202000195
90. X. Chen, H. Ji, Z. Rao, L. Yuan, Y. Shen et al., Insight into the fading mechanism of the solid-conversion sulfur cathodes and designing long cycle lithium–sulfur batteries. Adv. Energy Mater. **12**, 2102774 (2022). https://doi.org/10.1002/aenm.202102774
91. J. Sun, Y. Liu, L. Liu, J. Bi, S. Wang et al., Interface engineering toward expedited Li_2S deposition in lithium-sulfur batteries: a critical review. Adv. Mater. **35**, e2211168 (2023). https://doi.org/10.1002/adma.202211168
92. W.-G. Lim, S. Kim, C. Jo, J. Lee, A comprehensive review of materials with catalytic effects in Li-S batteries: enhanced redox kinetics. Angew. Chem. Int. Ed. **58**, 18746–18757 (2019). https://doi.org/10.1002/anie.201902413
93. L. Kong, J.-X. Chen, H.-J. Peng, J.-Q. Huang, W. Zhu et al., Current-density dependence of Li_2S/Li_2S_2 growth in lithium–sulfur batteries. Energy Environ. Sci. **12**, 2976–2982 (2019). https://doi.org/10.1039/c9ee01257e

94. M. Sadd, S. De Angelis, S. Colding-Jørgensen, D. Blanchard, R.E. Johnsen et al., Visualization of dissolution-precipitation processes in lithium–sulfur batteries. Adv. Energy Mater. **12**, 2103126 (2022). https://doi.org/10.1002/aenm.202103126
95. Z. Guan, X. Chen, F. Chu, R. Deng, S. Wang et al., Low concentration electrolyte enabling anti-clustering of lithium polysulfides and 3D-growth of Li_2S for low temperature Li–S conversion chemistry. Adv. Energy Mater. **13**, 2302850 (2023). https://doi.org/10.1002/aenm.202302850
96. R. Xu, J. Lu, K. Amine, Progress in mechanistic understanding and characterization techniques of Li-S batteries. Adv. Energy Mater. **5**, 1500408 (2015). https://doi.org/10.1002/aenm.201500408
97. S. Zhang, K. Ueno, K. Dokko, M. Watanabe, Recent advances in electrolytes for lithium–sulfur batteries. Adv. Energy Mater. **5**, 1500117 (2015). https://doi.org/10.1002/aenm.201500117
98. Y.-W. Song, J.-L. Qin, C.-X. Zhao, M. Zhao, L.-P. Hou et al., The formation of crystalline lithium sulfide on electrocatalytic surfaces in lithium–sulfur batteries. J. Energy Chem. **64**, 568–573 (2022). https://doi.org/10.1016/j.jechem.2021.05.023
99. L. Peng, Z. Wei, C. Wan, J. Li, Z. Chen et al., A fundamental look at electrocatalytic sulfur reduction reaction. Nat. Catal. **3**, 762–770 (2020). https://doi.org/10.1038/s41929-020-0498-x
100. W. Ren, W. Ma, S. Zhang, B. Tang, Recent advances in shuttle effect inhibition for lithium sulfur batteries. Energy Storage Mater. **23**, 707–732 (2019). https://doi.org/10.1016/j.ensm.2019.02.022
101. Z. Shi, Y. Ding, Q. Zhang, J. Sun, Electrocatalyst modulation toward bidirectional sulfur redox in Li–S batteries: from strategic probing to mechanistic understanding. Adv. Energy Mater. **12**, 2201056 (2022). https://doi.org/10.1002/aenm.202201056
102. B. Yue, L. Wang, N. Zhang, Y. Xie, W. Yu et al., Dual-confinement effect of nanocages@nanotubes suppresses polysulfide shuttle effect for high-performance lithium–sulfur batteries. Small **20**, 2308603 (2024). https://doi.org/10.1002/smll.202308603
103. S.-Y. Lang, R.-J. Xiao, L. Gu, Y.-G. Guo, R. Wen et al., Interfacial mechanism in lithium-sulfur batteries: how salts mediate the structure evolution and dynamics. J. Am. Chem. Soc. **140**, 8147–8155 (2018). https://doi.org/10.1021/jacs.8b02057
104. W. Li, K. Chen, Q. Xu, X. Li, Q. Zhang et al., Mo_2C/C hierarchical double-shelled hollow spheres as sulfur host for advanced Li-S batteries. Angew. Chem. Int. Ed. **60**, 21512–21520 (2021). https://doi.org/10.1002/anie.202108343
105. A. Kraytsberg, Y. Ein-Eli, Higher, stronger, better… A review of 5 volt cathode materials for advanced lithium-ion batteries. Adv. Energy Mater. **2**, 922–939 (2012). https://doi.org/10.1002/aenm.201200068
106. X. Chen, Z. Miao, X. Zhang, L. Yuan, Y. Huang et al., Optimizing the operation strategy of solid-conversion sulfur cathodes for achieving high total capacity contribution throughout the lifespan. J. Power. Sources **543**, 231837 (2022). https://doi.org/10.1016/j.jpowsour.2022.231837
107. Z. Wu, S.-M. Bak, Z. Shadike, S. Yu, E. Hu et al., Understanding the roles of the electrode/electrolyte interface for enabling stable Li‖Sulfurized polyacrylonitrile batteries. ACS Appl. Mater. Interfaces **13**, 31733–31740 (2021). https://doi.org/10.1021/acsami.1c07903
108. M. Liu, D. Zhou, Y.-B. He, Y. Fu, X. Qin et al., Novel gel polymer electrolyte for high-performance lithium–sulfur batteries. Nano Energy **22**, 278–289 (2016). https://doi.org/10.1016/j.nanoen.2016.02.008
109. X. Xing, Y. Li, X. Wang, V. Petrova, H. Liu et al., Cathode electrolyte interface enabling stable Li–S batteries. Energy Storage Mater. **21**, 474–480 (2019). https://doi.org/10.1016/j.ensm.2019.06.022
110. R. Cao, J. Chen, K.S. Han, W. Xu, D. Mei et al., Effect of the anion activity on the stability of Li metal anodes in lithium-sulfur batteries. Adv. Funct. Mater. **26**, 3059–3066 (2016). https://doi.org/10.1002/adfm.201505074
111. H. Kim, F. Wu, J.T. Lee, N. Nitta, H.-T. Lin et al., In situ formation of protective coatings on sulfur cathodes in lithium batteries with LiFSI-based organic electrolytes. Adv. Energy Mater. **5**, 1401792 (2015). https://doi.org/10.1002/aenm.201401792
112. J. Wang, S. Cheng, L. Li, L. Jia, J. Wu et al., Robust interfacial engineering construction to alleviate polysulfide shuttling in metal sulfide electrodes for achieving fast-charge high-capacity lithium storages. Chem. Eng. J. **446**, 137291 (2022). https://doi.org/10.1016/j.cej.2022.137291
113. Y. Xiao, B. Han, Y. Zeng, S.-S. Chi, X. Zeng et al., New lithium salt forms interphases suppressing both Li dendrite and polysulfide shuttling. Adv. Energy Mater. **10**, 1903937 (2020). https://doi.org/10.1002/aenm.201903937
114. Z. Shen, W. Zhang, S. Mao, S. Li, X. Wang et al., Tailored electrolytes enabling practical lithium–sulfur full batteries *via* interfacial protection. ACS Energy Lett. **6**, 2673–2681 (2021). https://doi.org/10.1021/acsenergylett.1c01091
115. C.-D. Qiu, Y. Hu, K. Cao, X. Wu, B.-H. Huang et al., Engineering peculiar cathode electrolyte interphase toward sustainable and high-rate Li–S batteries. Adv. Energy Mater. **13**, 2300229 (2023). https://doi.org/10.1002/aenm.202300229
116. H. Pan, K.S. Han, M.H. Engelhard, R. Cao, J. Chen et al., Addressing passivation in lithium–sulfur battery under lean electrolyte condition. Adv. Funct. Mater. **28**, 1707234 (2018). https://doi.org/10.1002/adfm.201707234
117. F. Liu, C. Zong, L. He, Z. Li, B. Hong et al., Improving the electrochemical performance of lithium-sulfur batteries by interface modification with a bifunctional electrolyte additive. Chem. Eng. J. **443**, 136489 (2022). https://doi.org/10.1016/j.cej.2022.136489
118. Y. Liu, Y. Pan, J. Ban, T. Li, X. Jiao et al., Promoted rate and cycling capability of Li–S batteries enabled by targeted selection of co-solvent for the electrolyte. Energy Storage Mater. **25**, 131–136 (2020). https://doi.org/10.1016/j.ensm.2019.10.022

 https://doi.org/10.1007/s40820-024-01573-4

119. Z. Li, Y. Zhou, Y. Wang, Y.-C. Lu, Solvent-mediated Li_2S electrodeposition: a critical manipulator in lithium–sulfur batteries. Adv. Energy Mater. **9**, 1802207 (2019). https://doi.org/10.1002/aenm.201802207
120. H. Chu, H. Noh, Y.-J. Kim, S. Yuk, J.-H. Lee et al., Achieving three-dimensional lithium sulfide growth in lithium-sulfur batteries using high-donor-number anions. Nat. Commun. **10**, 188 (2019). https://doi.org/10.1038/s41467-018-07975-4
121. J. Jung, H. Chu, I. Kim, D.H. Lee, G. Doo et al., Confronting sulfur electrode passivation and Li metal electrode degradation in lithium-sulfur batteries using thiocyanate anion. Adv. Sci. **10**, e2301006 (2023). https://doi.org/10.1002/advs.202301006
122. D. Tian, X. Song, Y. Qiu, X. Sun, B. Jiang et al., Heterogeneous mediator enabling three-dimensional growth of lithium sulfide for high-performance lithium–sulfur batteries. Energy Environ. Mater. **5**, 1214–1221 (2022). https://doi.org/10.1002/eem2.12236
123. J.-L. Yang, D.-Q. Cai, X.-G. Hao, L. Huang, Q. Lin et al., Rich heterointerfaces enabling rapid polysulfides conversion and regulated Li_2S deposition for high-performance lithium-sulfur batteries. ACS Nano **15**, 11491–11500 (2021). https://doi.org/10.1021/acsnano.1c01250
124. R. Xiao, T. Yu, S. Yang, K. Chen, Z. Li et al., Electronic structure adjustment of lithium sulfide by a single-atom copper catalyst toward high-rate lithium-sulfur batteries. Energy Storage Mater. **51**, 890–899 (2022). https://doi.org/10.1016/j.ensm.2022.07.024
125. M. Zhao, H.-J. Peng, J.-Y. Wei, J.-Q. Huang, B.-Q. Li et al., Dictating high-capacity lithium–sulfur batteries through redox-mediated lithium sulfide growth. Small Meth. **4**, 1900344 (2020). https://doi.org/10.1002/smtd.201900344
126. J. Song, T. Xu, M.L. Gordin, P. Zhu, D. Lv et al., Nitrogen-doped mesoporous carbon promoted chemical adsorption of sulfur and fabrication of high-areal-capacity sulfur cathode with exceptional cycling stability for lithium-sulfur batteries. Adv. Funct. Mater. **24**, 1243–1250 (2014). https://doi.org/10.1002/adfm.201302631
127. J.G. Kim, Y. Noh, Y. Kim, Highly reversible lithium-sulfur batteries with nitrogen-doped carbon encapsulated sulfur cathode and nitrogen-doped carbon-coated ZnS anode. Chem. Eng. J. **435**, 131339 (2022). https://doi.org/10.1016/j.cej.2021.131339
128. R. Li, H. Shen, E. Pervaiz, M. Yang, Facile in situ nitrogen-doped carbon coated iron sulfide as green and efficient adsorbent for stable lithium–sulfur batteries. Chem. Eng. J. **404**, 126462 (2021). https://doi.org/10.1016/j.cej.2020.126462
129. W. Qi, W. Jiang, F. Xu, J. Jia, C. Yang et al., Improving confinement and redox kinetics of polysufides through hollow NC@CeO_2 nanospheres for high-performance lithium-sulfur batteries. Chem. Eng. J. **382**, 122852 (2020). https://doi.org/10.1016/j.cej.2019.122852
130. Q. Wang, Z.-B. Wang, R. Li, H. Liu, M. Yang et al., Flower-like nitrogen-oxygen-doped carbon encapsulating sulfur composite synthesized via in situ oxidation approach. Chem. Eng. J. **345**, 271–279 (2018). https://doi.org/10.1016/j.cej.2018.03.179
131. F. Wu, Y.-S. Ye, J.-Q. Huang, T. Zhao, J. Qian et al., Sulfur nanodots stitched in 2D "bubble-like" interconnected carbon fabric as reversibility-enhanced cathodes for lithium-sulfur batteries. ACS Nano **11**, 4694–4702 (2017). https://doi.org/10.1021/acsnano.7b00596
132. R. Zhe, T. Zhu, X. Wei, Y. Ren, C. Qing et al., Graphene oxide wrapped hollow mesoporous carbon spheres as a dynamically bipolar host for lithium–sulfur batteries. J. Mater. Chem. A **10**, 24422–24433 (2022). https://doi.org/10.1039/d2ta06686f
133. P. Yu, L.-X. Feng, D.-C. Ma, X.-R. Sun, J.-K. Pei et al., Template-free self-caging nanochemistry for large-scale synthesis of sulfonated-graphene@sulfur nanocage for long-life lithium-sulfur batteries. Adv. Funct. Mater. **31**, 2008652 (2021). https://doi.org/10.1002/adfm.202008652
134. H. Jiang, X.-C. Liu, Y. Wu, Y. Shu, X. Gong et al., Metal-organic frameworks for high charge-discharge rates in lithium-sulfur batteries. Angew. Chem. Int. Ed. **57**, 3916–3921 (2018). https://doi.org/10.1002/anie.201712872
135. G. Wen, X. Zhang, Y. Sui, K. Rao, J. Liu et al., PPy-encapsulated *Hydrangea*-type 1T MoS_2 microspheres as catalytic sulfur hosts for long-life and high-rate lithium-sulfur batteries. Chem. Eng. J. **430**, 133041 (2022). https://doi.org/10.1016/j.cej.2021.133041
136. T. Wu, G. Sun, W. Lu, L. Zhao, A. Mauger et al., A polypyrrole/black-TiO_2/S double-shelled composite fixing polysulfides for lithium-sulfur batteries. Electrochim. Acta **353**, 136529 (2020). https://doi.org/10.1016/j.electacta.2020.136529
137. P. Zhu, J. Zhu, C. Yan, M. Dirican, J. Zang et al., In situ polymerization of nanostructured conductive polymer on 3D sulfur/carbon nanofiber composite network as cathode for high-performance lithium–sulfur batteries. Adv. Mater. Interfaces **5**, 1701598 (2018). https://doi.org/10.1002/admi.201701598
138. W. Li, Q. Zhang, G. Zheng, Z.W. Seh, H. Yao et al., Understanding the role of different conductive polymers in improving the nanostructured sulfur cathode performance. Nano Lett. **13**, 5534–5540 (2013). https://doi.org/10.1021/nl403130h
139. B. Long, Z. Qiao, J. Zhang, S. Zhang, M.-S. Balogun et al., Polypyrrole-encapsulated amorphous Bi_2S_3 hollow sphere for long life sodium ion batteries and lithium–sulfur batteries. J. Mater. Chem. A **7**, 11370–11378 (2019). https://doi.org/10.1039/c9ta01358j
140. P. Geng, S. Cao, X. Guo, J. Ding, S. Zhang et al., Polypyrrole coated hollow metal–organic framework composites for lithium–sulfur batteries. J. Mater. Chem. A **7**, 19465–19470 (2019). https://doi.org/10.1039/c9ta05812e
141. H. Dong, S. Qi, L. Wang, X. Chen, Y. Xiao et al., Conductive polymer coated layered double hydroxide as a novel sulfur reservoir for flexible lithium-sulfur batteries. Small **19**, e2300843 (2023). https://doi.org/10.1002/smll.202300843

142. J. Lei, X.-X. Fan, T. Liu, P. Xu, Q. Hou et al., Single-dispersed polyoxometalate clusters embedded on multilayer graphene as a bifunctional electrocatalyst for efficient Li-S batteries. Nat. Commun. **13**, 202 (2022). https://doi.org/10.1038/s41467-021-27866-5
143. B. Qin, Q. Wang, W. Yao, Y. Cai, Y. Chen et al., Heterostructured Mn_3O_4-MnS multi-shelled hollow spheres for enhanced polysulfide regulation in lithium–sulfur batteries. Energy Environ. Mater. **6**, e12475 (2023). https://doi.org/10.1002/eem2.12475
144. Y. Ren, J. Hu, H. Zhong, L. Zhang, Multiple core–shelled sulfur composite based on spherical double-layered hollow carbon and PEDOT:PSS as cathode for lithium–sulfur batteries. J. Alloys Compd. **837**, 155498 (2020). https://doi.org/10.1016/j.jallcom.2020.155498
145. Y. Zhang, H.W. Song, K.R. Crompton, X. Yang, K. Zhao et al., A sulfur cathode design strategy for polysulfide restrictions and kinetic enhancements in Li-S batteries through oxidative chemical vapor deposition. Nano Energy **115**, 108756 (2023). https://doi.org/10.1016/j.nanoen.2023.108756
146. Y. Zhang, C.S. Kim, H.W. Song, S.-J. Chang, H. Kim et al., Ultrahigh active material content and highly stable Ni-rich cathode leveraged by oxidative chemical vapor deposition. Energy Storage Mater. **48**, 1–11 (2022). https://doi.org/10.1016/j.ensm.2022.03.001
147. F. Shi, J. Yu, C. Chen, S.P. Lau, W. Lv et al., Advances in understanding and regulation of sulfur conversion processes in metal–sulfur batteries. J. Mater. Chem. A **10**, 19412–19443 (2022). https://doi.org/10.1039/d2ta02217f
148. S. Deng, T. Guo, J. Heier, C.J. Zhang, Unraveling polysulfide's adsorption and electrocatalytic conversion on metal oxides for Li-S batteries. Adv. Sci. **10**, e2204930 (2023). https://doi.org/10.1002/advs.202204930
149. X. Wang, N. Deng, L. Wei, Q. Yang, H. Xiang et al., Recent progress in high-performance lithium sulfur batteries: the emerging strategies for advanced separators/electrolytes based on nanomaterials and corresponding interfaces. Chem **16**, 2852–2870 (2021). https://doi.org/10.1002/asia.202100765
150. Y. Li, J. Liu, X. Wang, X. Zhang, N. Chen et al., $CoFe_2O_4$@rGO as a separator coating for advanced lithium–sulfur batteries. Small Sci. **3**, 2300045 (2023). https://doi.org/10.1002/smsc.202300045
151. B. Zhang, C. Luo, Y. Deng, Z. Huang, G. Zhou et al., Optimized catalytic WS_2–WO_3 heterostructure design for accelerated polysulfide conversion in lithium–sulfur batteries. Adv. Energy Mater. **10**, 2000091 (2020). https://doi.org/10.1002/aenm.202000091
152. W. Feng, H. Yang, Z. Pu, L. Zhang, Study of CNTs-MoS_2/CeO_2 composites for lithium-sulfur battery performance. Ionics **28**, 2781–2791 (2022). https://doi.org/10.1007/s11581-022-04535-1
153. Z. Ma, Y. Liu, J. Gautam, W. Liu, A.N. Chishti et al., Embedding cobalt atom clusters in CNT-wired MoS_2 tube-in-tube nanostructures with enhanced sulfur immobilization and catalyzation for Li-S batteries. Small **17**, e2102710 (2021). https://doi.org/10.1002/smll.202102710
154. M. Yu, J. Ma, H. Song, A. Wang, F. Tian et al., Atomic layer deposited TiO_2 on a nitrogen-doped graphene/sulfur electrode for high performance lithium–sulfur batteries. Energy Environ. Sci. **9**, 1495–1503 (2016). https://doi.org/10.1039/C5EE03902A
155. Y. Kim, W.I. Kim, H. Park, J.S. Kim, H. Cho et al., Multifunctional polymeric phthalocyanine-coated carbon nanotubes for efficient redox mediators of lithium–sulfur batteries. Adv. Energy Mater. **13**, 2370095 (2023). https://doi.org/10.1002/aenm.202370095
156. W. Chen, Y. Hu, W. Lv, T. Lei, X. Wang et al., Lithiophilic montmorillonite serves as lithium ion reservoir to facilitate uniform lithium deposition. Nat. Commun. **10**, 4973 (2019). https://doi.org/10.1038/s41467-019-12952-6
157. X. Zhang, Y. Chen, F. Ma, X. Chen, B. Wang et al., Regulating Li uniform deposition by lithiophilic interlayer as Li-ion redistributor for highly stable lithium metal batteries. Chem. Eng. J. **436**, 134945 (2022). https://doi.org/10.1016/j.cej.2022.134945
158. J. Wang, L. Wang, Z. Li, J. Bi, Q. Shi et al., Recent advances of metal groups and their heterostructures as catalytic materials for lithium-sulfur battery cathodes. J. Electron. Mater. **52**, 3526–3548 (2023). https://doi.org/10.1007/s11664-023-10355-4
159. R. Wang, C. Luo, T. Wang, G. Zhou, Y. Deng et al., Bidirectional catalysts for liquid–solid redox conversion in lithium-sulfur batteries. Adv. Mater. **32**, e2000315 (2020). https://doi.org/10.1002/adma.202000315
160. L. Jiao, C. Zhang, C. Geng, S. Wu, H. Li et al., Capture and catalytic conversion of polysulfides by in situ built TiO_2-MXene heterostructures for lithium–sulfur batteries. Adv. Energy Mater. **9**, 1900219 (2019). https://doi.org/10.1002/aenm.201900219
161. S. Nam, J. Kim, V.H. Nguyen, M. Mahato, S. Oh et al., Collectively exhaustive MXene and graphene oxide multilayer for suppressing shuttling effect in flexible lithium sulfur battery. Adv. Mater. Technol. **7**, 2101025 (2022). https://doi.org/10.1002/admt.202101025
162. H. Wang, S.-A. He, Z. Cui, C. Xu, J. Zhu et al., Enhanced kinetics and efficient activation of sulfur by ultrathin MXene coating S-CNTs porous sphere for highly stable and fast charging lithium-sulfur batteries. Chem. Eng. J. **420**, 129693 (2021). https://doi.org/10.1016/j.cej.2021.129693
163. F. Yin, Q. Jin, H. Gao, X. Zhang, Z. Zhang, A strategy to achieve high loading and high energy density Li-S batteries. J. Energy Chem. **53**, 340–346 (2021). https://doi.org/10.1016/j.jechem.2020.05.014
164. Q. Zhao, Q. Zhu, Y. Liu, B. Xu, Status and prospects of MXene-based lithium–sulfur batteries. Adv. Funct. Mater. **31**, 2100457 (2021). https://doi.org/10.1002/adfm.202100457
165. T. Zhang, L. Zhang, Y. Hou, MXenes: synthesis strategies and lithium-sulfur battery applications. eScience **2**, 164–182 (2022). https://doi.org/10.1016/j.esci.2022.02.010

 https://doi.org/10.1007/s40820-024-01573-4

166. M. He, X. Li, X. Yang, C. Wang, M.L. Zheng et al., Realizing solid-phase reaction in Li–S batteries *via* localized high-concentration carbonate electrolyte. Adv. Energy Mater. **11**, 2101004 (2021). https://doi.org/10.1002/aenm.202101004
167. H. Li, X. Wu, S. Jiang, Q. Zhang, Y. Cao et al., A high-loading and cycle-stable solid-phase conversion sulfur cathode using edible fungus slag-derived microporous carbon as sulfur host. Nano Res. **16**, 8360–8367 (2023). https://doi.org/10.1007/s12274-022-5156-y
168. L. Yu, S. Chen, H. Lee, L. Zhang, M.H. Engelhard et al., A localized high-concentration electrolyte with optimized solvents and lithium difluoro(oxalate)borate additive for stable lithium metal batteries. ACS Energy Lett. **3**, 2059–2067 (2018). https://doi.org/10.1021/acsenergylett.8b00935
169. J. Chen, H. Lu, X. Zhang, Y. Zhang, J. Yang et al., Electrochemical polymerization of nonflammable electrolyte enabling fast-charging lithium-sulfur battery. Energy Storage Mater. **50**, 387–394 (2022). https://doi.org/10.1016/j.ensm.2022.05.044
170. T. Ma, Y. Ni, D. Li, Z. Zha, S. Jin et al., Reversible solid–solid conversion of sulfurized polyacrylonitrile cathodes in lithium–sulfur batteries by weakly solvating ether electrolytes. Angew. Chem. Int. Ed. **135**, e202310761 (2023). https://doi.org/10.1002/ange.202310761
171. X. Li, M. Banis, A. Lushington, X. Yang, Q. Sun et al., A high-energy sulfur cathode in carbonate electrolyte by eliminating polysulfides via solid-phase lithium-sulfur transformation. Nat. Commun. **9**, 4509 (2018). https://doi.org/10.1038/s41467-018-06877-9
172. W. Guo, W. Zhang, Y. Si, D. Wang, Y. Fu et al., Artificial dual solid-electrolyte interfaces based on in situ organothiol transformation in lithium sulfur battery. Nat. Commun. **12**, 3031 (2021). https://doi.org/10.1038/s41467-021-23155-3
173. Y. Yi, W. Huang, X. Tian, B. Fang, Z. Wu et al., Graphdiyne-like porous organic framework as a solid-phase sulfur conversion cathodic host for stable Li-S batteries. ACS Appl. Mater. Interfaces **13**, 59983–59992 (2021). https://doi.org/10.1021/acsami.1c19484
174. X. Li, D. Liu, Z. Cao, Y. Liao, Z. Cheng et al., Uncovering the solid-phase conversion mechanism *via* a new range of organosulfur polymer composite cathodes for lithium-sulfur batteries. J. Energy Chem. **84**, 459–466 (2023). https://doi.org/10.1016/j.jechem.2023.05.052
175. X. Zhang, G. Hu, K. Chen, L. Shen, R. Xiao et al., Structure-related electrochemical behavior of sulfur-rich polymer cathode with solid-solid conversion in lithium-sulfur batteries. Energy Storage Mater. **45**, 1144–1152 (2022). https://doi.org/10.1016/j.ensm.2021.11.014
176. S. Zhou, J. Shi, S. Liu, G. Li, F. Pei et al., Visualizing interfacial collective reaction behaviour of Li-S batteries. Nature **621**, 75–81 (2023). https://doi.org/10.1038/s41586-023-06326-8
177. G.W. Sun, M.J. Jin, Q.Y. Liu, C.Y. Zhang, J.L. Pan et al., Unveiling the enhancement essence on Li_2S deposition by the polarized topological β-polyvinylidene fluoride: beyond built-in electric field effect. Chem. Eng. J. **453**, 139752 (2023). https://doi.org/10.1016/j.cej.2022.139752
178. Z. Zhang, Z. Fang, Y. Xiang, D. Liu, Z. Xie et al., Cellulose-based material in lithium-sulfur batteries: a review. Carbohydr. Polym. **255**, 117469 (2021). https://doi.org/10.1016/j.carbpol.2020.117469
179. L. Dong, J. Liu, D. Chen, Y. Han, Y. Liang et al., Suppression of polysulfide dissolution and shuttling with glutamate electrolyte for lithium sulfur batteries. ACS Nano **13**, 14172–14181 (2019). https://doi.org/10.1021/acsnano.9b06934
180. B. Wang, L. Wang, B. Zhang, S. Zeng, F. Tian et al., Niobium diboride nanoparticles accelerating polysulfide conversion and directing Li_2S nucleation enabled high areal capacity lithium-sulfur batteries. ACS Nano **16**, 4947–4960 (2022). https://doi.org/10.1021/acsnano.2c01179
181. L.C.H. Gerber, P.D. Frischmann, F.Y. Fan, S.E. Doris, X. Qu et al., Three-dimensional growth of Li_2S in lithium-sulfur batteries promoted by a redox mediator. Nano Lett. **16**, 549–554 (2016). https://doi.org/10.1021/acs.nanolett.5b04189
182. Y. Wu, Y. Feng, X. Qiu, F. Ren, J. Cen et al., Construction of polypyrrole-coated $CoSe_2$ composite material for lithium-sulfur battery. Nanomaterials **13**, 865 (2023). https://doi.org/10.3390/nano13050865
183. J.-L. Yang, S.-X. Zhao, X.-T. Zeng, Y.-M. Lu, G.-Z. Cao, Catalytic interfaces-enriched hybrid hollow spheres sulfur host for advanced Li–S batteries. Adv. Mater. Interfaces **7**, 1901420 (2020). https://doi.org/10.1002/admi.201901420
184. W. Bao, L. Liu, C. Wang, S. Choi, D. Wang et al., Facile synthesis of crumpled nitrogen-doped MXene nanosheets as a new sulfur host for lithium–sulfur batteries. Adv. Energy Mater. **8**, 1702485 (2018). https://doi.org/10.1002/aenm.201702485
185. J. Huang, M. Tao, W. Zhang, G. Zheng, L. Du et al., Realizing a "solid to solid" process via in situ cathode electrolyte interface (CEI) by solvent-in-salt electrolyte for Li-S batteries. Nano Res. **16**, 5018–5025 (2023). https://doi.org/10.1007/s12274-023-5443-2
186. L. Li, J.S. Nam, M.S. Kim, Y. Wang, S. Jiang et al., Sulfur–carbon electrode with PEO-LiFSI-PVDF composite coating for high-rate and long-life lithium–sulfur batteries. Adv. Energy Mater. **13**, 2302139 (2023). https://doi.org/10.1002/aenm.202302139
187. G. Li, X. Wang, M.H. Seo, M. Li, L. Ma et al., Chemisorption of polysulfides through redox reactions with organic molecules for lithium-sulfur batteries. Nat. Commun. **9**, 705 (2018). https://doi.org/10.1038/s41467-018-03116-z
188. C. Hu, H. Chen, Y. Shen, D. Lu, Y. Zhao et al., In situ wrapping of the cathode material in lithium-sulfur batteries. Nat. Commun. **8**, 479 (2017). https://doi.org/10.1038/s41467-017-00656-8